



Wildfires as part of the global carbon cycle: quantitative analysis using data assimilation



Douglas Kelley
Supervisors:
Wolfgang Knorr, Marko Scholze
Yiorgos Petropoulos



Abstract

Estimates for global and regional fire carbon emission vary greatly, due mainly to lack of studies and sensitivity of fire regimes to climate and vegetation composition. Fire thus represents a substantial uncertainty on the global carbon cycle, both for the present day and in the future. Wildfires may also be a substantial source of interannual variability in growth rate of atmospheric CO_2 , driven by interannual variations in Climate, dominated by ENSO. This is an initial report on a study exploring how to constraining the relative contributions of fire carbon emissions compared to other natural sources (i.e. heterotrophic respiration) on the global carbon cycle. This is achieved by developing a fire model Fire Statistical Emissions Global model (FISLING) coupled to the vegetation model BETHY, describing terrestrial vegetation processes affecting carbon fluxes. The couple FISLING/BETHY models are optimized using satellite remote sensing and atmospheric CO_2 data using the Carbon Cycle Data Assimilation System (CCDAS). The optimized model is used to explore the relative contributions of fire carbon emission sources to atmospheric CO_2 during El Niño or La Niña ENSO phases, and demonstrates: a significant increase in wildfire carbon emissions during El Niño phases; and a large global variation in ENSO effects on the terrestrial biosphere to act as a sink. The model qualitatively describes the fluctuations in flux through different seasons and interannual varying climate condition, particularly those governed by ENSO. Quantitatively, however, the fluxes are still some way from accurate, although the model is still being developed.

Acknowledgments

Thanks to my Supervisors, Marko Scholze & Wolfgang Knorr. Marko helped with some of the complexities of the CCDAS source code, and Wolfgang provided direction and suggestions of areas to study. Alice Hooker-Stroud helps with the Georeferencing and optimization problems. George (or Yiorgos?!) Petropoulos helped with all the software and programme installation, pointed me towards all the remote sensing datasets and was generally very helpful despite being busy with everything else and not really meant to be helping me. Thanks to the Earth System Science Msc class '08, for letting me bounce ideas off them, and anyone in the Quest office for my constant pestering.

Declaration

I declare this to be my own work, and any external material and information has been properly acknowledged.

Table of Contents

Abstract.....	i
Acknowledgements.....	ii
Declaration.....	ii
Table of Contents.....	iii
Glossary	iv
<i>abbreviation</i>	iv
<i>symbols</i>	v
1. Introduction.....	1
<i>Climate and fire management policy</i>	1
<i>ENSO, Climate Variability & Climate Change</i>	2
<i>Previous studies</i>	3
2. Models and Methods	5
<i>BETHY & CCDAS</i>	5
<i>The Model: FISSLING</i>	7
<i>a. Biomisation</i>	8
<i>b. Season Length</i>	10
<i>c. Carbon Fire Emissions</i>	12
<i>d. Mortality</i>	13
<i>Carbon Balance</i>	13
3, Data and parameter construction	14
<i>Satellite Data</i>	14
<i>a. Fuel threshold</i>	14
<i>b, Moisture of extinction</i>	15
<i>c. Burnt Fraction vs. thermal anomaly</i>	17
<i>d. Emission parameters</i>	24
4. Model Validation & Evaluation	27
5. Results	30
<i>Enso</i>	30
6. Discussion and Conclusion	34
7. References	35

Glossary

Abbreviations

AVHRR	Advanced Very High Resolution Radiometer (remote sensing instrument)
BETHY	Biosphere Energy Transfer Hydrology
C3/C4	different photosynthetic pathways
CCDAS	Carbon Cycle Data Assimilation system
DGVM	Dynamic Global Vegetation Model
ENSO Positive phase Negative phase Event	El Niño-Southern Oscillation Warmer than usual Eastern Pacific sea surface temperature/ decreased Pacific sea surface temperature gradient Warmer Western Pacific/ increased sea surface temperature gradient Either positive or negative ENSO phase
fAPAR	fraction of Absorbed Photosynthetically Active Radiation
FISLING	Fire Statistical Emissions Global model
GLOB_FIRM	Global FIRE Model
HPI	Human Footprint Index
IAV	InterAnnual Variability
IIASA	International Institute for Applied Systems Analysis
IPCC	Intergovernmental Panel on Climate Change
LAI	Leaf Area Index
LPJ	Lund–Potsdam–Jena model, a Dynamic Global Vegetation Model
MODIS	Moderate Resolution Imaging Spectroradiometer (remote sensing instrument)
NDVI	Normalized Difference Vegetation Index
NDWI	Normalized Difference Water Index
NPP	Net Primary Production

ONI	Oceanic Niño Index
PFT	Plant Functional Type
PFT cell	Part of a grid cell describing carbon balance for 1 of the cells' PFTs
SeaWiFS	Sea-viewing Wide Field-of-view Sensor (remote sensing instrument)
SEVIRI	Spinning Enhanced Visible & InfraRed Imager (remote sensing instrument)
SPITFIRE	
TM2	Transport Model-2

Symbols

A_j	Affinity score for a biome j
A_{nf}	Affinity score of the 'no fire' biome
$B, B(s)$ or $B(\underline{x}, t)$	Burnt fraction of cell (as a function of season length)
B_{λ_i, ϕ_k}	data point from emissions database describing burnt fraction with a upper boundary latitude of λ_i and a left hand boundary longitude of ϕ_k
$Bm_{j,v}$	Biome matrix entry for biome j & PFT i
B_{obs}	Burnt fraction from satellite observation in cost function used to determine moisture of extinction parameters
B_{sim, m_e}	Burnt fraction simulated by FISSLING using moisture of extinction values, m_e .
B_v	Burnt fraction of PFT v with a cell.
$C_{BE,j}$	Emission Parameter for biome j
$C_{PE,v}$	Emissions Parameter for PFT v

$C_{J,i}$	Parameter describing conversation from season length to burnt fraction for a dominant biome, J
$C_{m,v}$	mortality parameter for PFT v
D	day number within a month
D_i	intermediate function used when georeferencing a pixel in thermal anomalies image
E_v	emissions for PFT v in a grid cell
FL	Fuel load of a cell
$f(S)$	exponential term in the season length to burnt fraction equation
fr	fractional length between corners/indeterminate points of intermediate point/pixel on the thermal anomalies data image
ΔL_+	litter production. Additions to the litter layer through dying vegetation, deciduous leaf loss and fire mortality
ΔL_-	litter loss, through fast respiration, fire emissions, and loss to soil layer
$m_{e,j}$	moisture of extinction for biome j .
m_d	moisture content of a cell on day d
m_M	moisture content of a cell during month M
n_b	number of biomes (9 in this study)
n_g	number of grid cells in model
n_M	number of days in month M
n_{Stw}	number of weather station
n_{Sty_i}	number of years historical climate data is based on at weather station i .
n_v	number of different PFTs in cell
n_{px}	height and breadth in pixels of a thermal anomalies data image, normally 1200.
$PFT_{frac,v}$	-Fraction of vegetation in a cell of type i

P_h	number of obscured or water pixels in the study region section of a thermal anomalies image
$p(m_d)$	probability of a fire occurring on day d with moisture m_d
pf_v	fraction of vegetation in a cell in PFT v.
P_h	total number of pixels in a study region part of a thermal anomalies image
R	intermediate function when calculating season length, describing the amount of unobscured pixels in a thermal anomalies image relative to a perfect equatorial image
S	(modified)months season length
S_o	observed season length
St_i	Historical precipitation at weather station i .
$TA_{i,k}$	Thermal anomalies pixel i down and k in on the image
W	Precipitation
X, Y, Z	intermediate functions used when georeferencing a pixel in thermal anomalies
α	conversion factor from fire pixel count to burnt area
λ_1 & λ_2	latitude of the corners/midway points of a thermal anomalies image. Either corresponding to top left & top right, bottom left & bottom right or intermediate points along the side of the image depending on the use of the equation
λ_a	latitude of the upper boundary of a study region
λ_b	latitude of the lower boundary of a study region
λ_c	latitude of the mid point of a study region
$\Delta\lambda_{rg}$	difference is latitude between upper and lower boundary of a study region. Normally equals 2 deg.
ϕ_1 & ϕ_2	longitude of corners/,midway points. See ' λ_1 & λ_2 ' above.
φ	cost function to be minimized when calculating moisture of extinction using modeled and observed burnt fraction

1. Introduction

The terrestrial biosphere, as well as having local ecological and economic significance, is also important at the global scale. In the face of increasing CO_2 concentrations in the atmosphere, it acts as a major sink of carbon (Denman and Brasseur, 2007), reducing the effect of anthropogenic carbon dioxide emissions. Various disturbances of those ecosystems not only alter their composition (Loreau et al, 2001; bond et al, 2005), but also influence how ecosystems impact on the carbon cycle. Wildfires in particular directly alter the carbon cycle through their emission of greenhouse gases (particularly CO_2), which would otherwise be released much more slowly via soil respiration.

Current estimates for the contribution to atmospheric CO_2 by wildfires vary greatly (e.g. $3.53 \pm 1.17 \text{ PgC yr}^{-1}$ van der Werf et al, 2004), and are normally only studied on a regional scale (e.g., Conard & Ivanova, 1997; Bond-Lamberty et al, 2004; Wiedinmyer et al, 2007). Different biomes have different carbon stores (i.e wood, roots and soil; Norby et al, 2005) and fire regimes. Some biomes, such as savana grasslands, rely on fire in order to spur new growth (Bond et al, 2005) by outcompeteing other vegetation tyopes (BOND et al, 2003). This affects the succession after the fire disturbance has occurred, and therefore produces a knock-on effect on possible carbon sinks of the region. All these factors contribute to the uncertainty that lies in occurrence and intensity of fires and contribution to ecosystem dynamics across different regions and biomes (Langenfelds, 2002). It is important to understand and quantify the effects of wildfires on the carbon cycle for several reasons.

Climate and fire management policy

International agreements and regulations on climate change, such as the Kyoto protocol, allow changes in land-use and forestry activities to contribute to emission reduction commitments (Kyoto Protocol, 1998). This includes fire management in relation to both natural and anthropogenic fires (Jonas et al, 1999). Accurate estimates of wildfire occurrence, intensity and CO_2 release is therefore important for international protocols such as Kyoto, and will be vitally important when formulating its successor. IIASA's Sustainable Boreal Forest Resources (Shvidenko et al, 1995) has already undertaken work on a full carbon accounting of Siberian forests (which account for 20% of the world's carbon stored in forest vegetation) on behalf of Russia including looking at forest and

forest fire management to help meet their reduction commitments. Studies are also coming out for carbon sequestration in Europe forests by proscribed burning (e.g. Narayan et al, 2007).

ENSO, Climate Variability & Climate Change

El Niño-Southern Oscillation (ENSO) is a global coupled ocean-atmosphere phenomenon, linked to fluctuations in the Pacific Ocean seas surface temperature gradient. The normal conditions over the southern and equatorial Pacific is cooler, upwelling in Eastern Pacific (of the South American Coast), to warmer waters in the Western, Asian Pacific (Vecchi & Harrison, 2000) El Niño (ENSO positive phase) and La Niña (ENSO negative phase) are important temperature fluctuations in this gradient surface waters, with positive phase reflecting in a warmer Eastern Pacific, and a more uniform gradient (Rasmusson & Wallace, 1983), while the negative phase is displayed in a stronger gradient, with cooler eastern and warmer western temperatures (Rasmusson & Wallace, 1983).

ENSO is associated with floods, droughts, and other ecosystem disturbances in a range of locations around the world (Barber & Chávez, 1986), particularly in tropical ecosystems (Jianhua & Slingo, 1995; Williamson et al, 2001; Byron & Shepherd, 1998) and is the most prominent inter-annual variability in weather and climate around the world (about 3 to 8 years; Cane, 1986; Glantz, 1991; Diaz & Markgraf, 1993). This makes predicting its timing and effects of high interest.

Interannual CO_2 concentrations have been shown to vary in relation to the ENSO (Keeling et al. 1989), with increased growth rates during ENSO's positive phase. In fact, ENSO correlates with the largest proportion of interannual variability (IAV) in CO_2 growth rate (Keeling et al., 1989). It is widely accepted that the source of this increase is the terrestrial biosphere (Jones & Cox 2005), as the oceans, which increase their sink during ENSO's positive phase (Zeng et al. 2005), is relatively small compared to terrestrial processes (Lee et al, 1998; Barttle et al, 2000; Bousquet et al, 2000).

It still remains unclear, however, what the specific and relative contributions of terrestrial processes are. Understanding these processes will help understand how the terrestrial biosphere will adapt to changing climates. Two main hypotheses exist that link the change in precipitation to CO_2 variability, and are related to reduction in precipitation during the ENSO positive (Lyon 2004, Knorr et al. 2005b). In the first hypothesis, less moisture availability causes subtle changes in photosynthesis, and thus Net Primary Production (NPP; as a sink) and plant and soil respiration (as a source). This is well supported by biosphere models (e.g. Knorr 2000; Knorr et al. 2005b; Zeng et al. 2005) and tree ring observations (Clark et al. 2003). The second, and a target of this study, is that reduced

precipitation reduces moisture content of fuel layer, increasing fire frequency and magnitude (Wooster et al. 1998). Indonesian fire in 97/98 El Niño event, and CO concentrations (caused by incomplete combustion; Langenfelds et al. 2002) support this hypothesis.

Both are likely to contribute somewhat to the changes in CO₂ concentration growth, with different ecosystems and biomes behaving in different ways. Again, contribution to interannual variability of CO₂ growth rate from fires in El Niño years varies drastically. For example, van der Werf et al (2004) estimated wildfires accounted for 66% ± 22% of 1997-2001 El Niño CO₂ variability. Contribution from NPP and heterotrophic respiration due to drought conditions remain largely unquantified and uncertain. For example, temperate ecosystems, El Niño conditions increase the rate of NPP and carbon uptake in hardwood forests (Goulden et al, 1996), whereas string drought in Europe in 2003 led to carbon loss (Ciais et al 2005).

Although much uncertainty still remains (Merryfield, 2006; Collins et al, 2005), changes in occurrence of ENSO positive phase have already be attributed to climate change (Trenberth and Hoar, 1996; Collins et al, 2005), with increases of likelihood and severity of El Niño and reduction in La Niño phases (Trenberth and Hoar, 1997 IPCC, 2007), and a slightly shortened cycle (Merryfield; 2006). This would result in decrease in moisture in many equatorial biomes, including tropical forests, which account for upto 40% of terrestrial carbon stores (Grace et al, 2002). As these forests have had little disturbance from natural fires over the past few thousand years (Sanford et al, 1985; Turcotte et al, 1998), a change in fire regime is likely to have a large effect on the ecosystem composition and its effectiveness as a sink, possibly turning tropical rainforests into a source (Cox et al, 2004; IPCC, 2007).

Previous studies

Although many models exist describing the propagation of fires and other disturbances, and their effects on local ecosystems, most are on a regional scale (Albini, 1976; Keane et al., 1996; Trunfio, 2004) and there are very few models that predict global fire activity and emissions. One such model is Glob-FIRM, incorporated into the Dynamic Global Vegetation Model Lund–Potsdam–Jena (LPJ; Sitch et al, 2000; Smith et al, 2001). LPJ describes key ecosystem processes, including vegetation establishment, resource competition, growth and mortality, through 9 different PFTs defined by plant physiological (eg C3/C4 photosynthesis), phenological (eg deciduous or evergreen) and physiognomic (tree/grass ect) and with climate and soil texture inputs. GLOB_FIRM simulates

global fire disturbance patterns using a small number of inputs and parameters (Thonicke et al, 2001). This model's predictions represent most biomes accurately, but has only been validated against a few locally based observations, and do not correspond with all regions such as boreal Siberia and semi-arid Africa. In Siberian boreal forest, different distribution patterns of fire severity across the landscape caused by varying permafrost can produce fourfold differences in carbon release (Conard & Ivanova, 1997) whereas in Savanna and arid Africa, availability and type of fire fuels, such as dead litter or living fuel at different thicknesses (Brown, 1981), are important determinants of fire potential.

Here we try not just to quantify the contribution of wildfires to the carbon cycle, but quantify some of corresponding problems and uncertainties, highlighted by Gob_FIRM, by using the modelling tool Carbon Cycle Data Assimilation System (CCDAS), built around the terrestrial biosphere ecosystem model, Biosphere Energy Transfer Hydrology model (BETHY) (Rayner, 2005; <http://www.ccdas.org>). This is used to assess the relative contribution of fire and heterotrophic respiration to CO₂ emissions during ENSO events.

2. Models and Methods

BETHY & CCDAS

To explore processes and to predict the behaviour of systems such as the carbon cycle, the most common approach is forward modeling of its most important processes. Although checked against other models and data sources, there is normally no formal data testing for these models¹⁰.

CCDAS solves this problem by optimizing the controlling parameters of the vegetation model, BETHY (Knorr, 2000), with respect to observations combined with prior, observational and process

(or model)

uncertainties. This

both constrains and

provides posterior

uncertainties for the

parameters that can

then be propagated

through the model

for assigning

uncertainties to

carbon cycle

predictions.

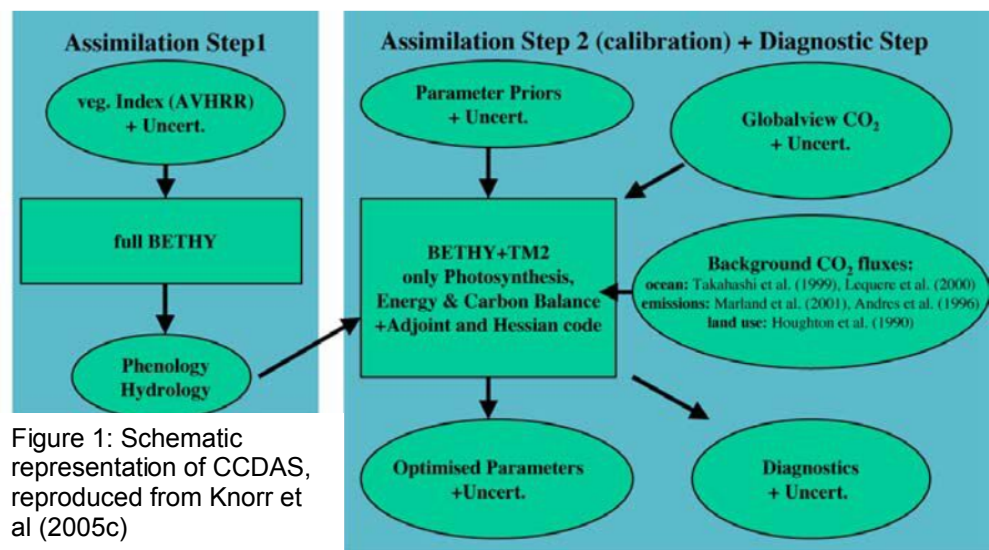


Figure 1: Schematic representation of CCDAS, reproduced from Knorr et al (2005c)

Figure 1 gives an overview of CCDAS (Knorr et al, 2005c). Using BETHY (Knorr, 1997), CCDAS carries out two assimilation steps. Step 1 (left hand box, figure 1) uses a variational approach to optimize parameters controlling soil moisture and phonology and hydrology within the BETHY model using the observed fraction of Absorbed Photo synthetically Active Radiant (fAPAR) provided by AVHRR satellite data (Knorr 1997, Knorr 2000). This is done by defining a cost function by the squared deviation of AVHRR observations and those predicted by BETHY (Rayner et al, 2005). For more details, see Knorr 1997 and Knorr & Schulz, 2001. For this study, an additional optimization step similar to this has been introduced to optimize fire related moisture parameters (see Methods, pg ??)

Step 2 uses a stripped down version of BETHY (carbon-BETHY), simulating photosynthesis, carbon and energy balance (Scholze, 2003; Rayner et al; 2005). Leaf Are Index (LAI) and plant available moisture quantifying phonology and hydrology respectively are provided for each grid cell by step 1.

Model concentrations of CO_2 are simulated by coupling carbon-BETHY to an atmospheric transport model, TM2 (Heimann, 1995). The TM2 Jacobean Matrix (Kaminiski et al, 1999) takes the role of an observational operator. CO_2 concentration data from GLOBALVIEW flask sampling network (GLOBALVIEW CO_2 , 2001) is used to assimilate atmospheric predicted CO_2 by applying the adjoint method and estimates (in this study) 70 parameters, all specified as control variables. This includes: 56 process-parameters, already part of CCDAS in previous studies (e.g. Knorr et al, 2005c, Raymer et al, 2005); 13 fire emission parameters from this study; and an initial condition parameter. The 56 parameters from previous studies are re-optimized along with the additional fire parameters. The inverse Hessian approximates the control variable's posterior uncertainties, combining the observational and model uncertainty. For more details on CCDAS optimization, refer to Rayner et al, 2005; Scholze 2003 and Kaminski et al 2002 & 2003.

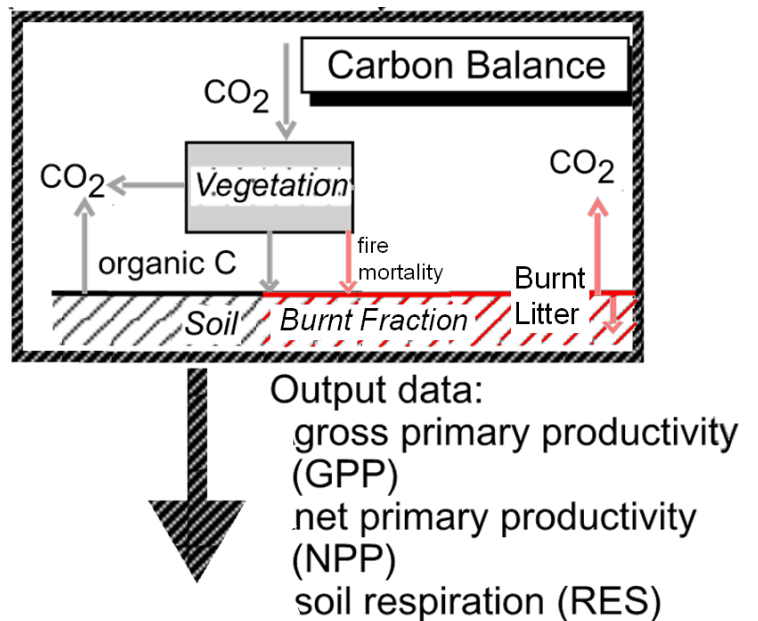


Figure 2: Adapted from Knorr (1997). Showing fluxes between different pools for BETHY (grey arrows) and FISSLING (pink arrows).

BETHY currently simulates the sources and sinks of CO_2 from global vegetation in the terrestrial biosphere. Run on either 2 by 2 degrees sized grid cells 'high resolution' or roughly 7.5deg (lat) by 10deg (lon) 'low resolution', both of which have been used in this study, it is driven by temperature, precipitation and solar incoming radiation. Foreword runs are coupled to a General Circulation Model (GCM). Each grid cell has a maximum of 3 prescribed and fixed PFT types and PFT fractional cover. Each PFT in each grid cell (PFT cell) has its own carbon balance between three main store: living plant layer; litter layer (for the fire model, also referred to as fuel load); and soil carbon store. This is done using parameters that describe local and global processes and functions such as photosynthesis, respiration and water loss for 13 different PFTs (figure 2). It is these parameters that are optimized using CCDAS. Each PFT cells carbon balance is calculated with fluxes from: live plant store to litter layer (litter production, equation 8); litter layer to soil carbon store and fast respiration to the atmosphere (litter loss, equation 8); and soil carbon store to

atmosphere through slow respiration. Fast and slow respiration are both sources of atmospheric CO_2 . Atmospheric CO_2 is taken up by vegetation through net primary production (NPP), which increases the size of the live carbon store. When used in CCDAS, respiration and NPP are fluxes fed to and from the TM2 transport model.

CCDAS offers an objective calibration against observation (Rayner, 2005), allowing quantifying of key processes in the carbon cycle (Knorr, 2005b). Up till now, BETHY, did not contain a prognostic fire model, and was therefore missing an important terrestrial process in its projections. Fire CO_2 emissions were instead lost in fast and slow respiration fluxes. This provides a major source of uncertainty in CO_2 source, including temporal and spatial disparity.

There are many factors that can be explored when considering wildfires as part of the global carbon cycle. Building on existing terrestrial models such as BETHY, a fire model will have to explore the effects that regional properties, such as vegetation (i.e. PFT) composition and fraction, fuel load, moisture and feedbacks (such as mortality and succession), have on fire disturbances, and how, in different biomes, with different partitionings between carbon stores, these properties affect ignition and occurrence, intensity, propagation size, and ultimately carbon release.

The Model: FISSLING

To link fire emissions to vegetation dynamics and the global carbon cycle, a global fire model, Fire Statistical Emissions Global model (FISSLING) has been developed and incorporated into terrestrial BETHY, using a similar approach to the Glob-FIRM model ran through LPJ (Thonicke et al, 2001). FISSLING needs to fulfill a number of requirements:

1. The processes that drive it must be general enough to be applicable across the globe;
2. It must be able to describe varying interactions different ecosystems/biomes have with their fire regimes;
3. It should describe the exchange between carbon stores (living matter, litter layer, soil and atmosphere) due to wildfire;
4. Work on a monthly timestep, using inputs available from BETHY;
5. Be able to distinguish emissions from wildfire and ecosystem respiration;
6. Directly comparable with available observations such as satellite observations of burnt fraction and fire emissions (Randerson et al, 2007; Van der Werf et al; 2006)

The input's that are used from BETHY are for each grid cell are:

- Monthly soil (inc. litter layer) moisture;
- Monthly fuel load (mass of the litter layer);
- Vegetation fraction for a maximum three different PFTs, predetermined on a grid-by grid basis by BETHY's inputs.

To achieve the requirements, burnt fraction, emissions and plant mortality (and hence carbon exchanges) are calculated as outputs for each cell from fuel load and moisture content through a series of steps:

1. As an initialization step, using vegetation fractions to calculate the biome of the grid cell;
2. From fuel load and soil moisture, calculating the length of the fire season each month;
3. Match the season length to a corresponding burnt fraction;
4. divide this burnt area amongst the cells different PFTs, and calculate vegetation mortality and carbon emissions;
5. Redistribute carbon accordingly around carbon stores, taking into account carbon (predominantly composed of CO_2) fire emissions and fire induced plant mortality.

1. Biomisation

The fire model calculates each step upto burnt fraction on a biome level. This is for two reasons. Firstly disturbance regimes can be affected by the mix and relative abundance of vegetation within the area, not just individual vegetation types (Chapin et al, 1997; Hobbes 2005); and secondly the model was constructed using satellite data (see below) at 2 degree resolution, too coarse to identify individual vegetation types. In future studies, or this may allow changes in fire regimes in individual cells by incorporating changes in PFT fractional composition through effects such as fire (and other disturbance/processes) mortality and succession. Here, however the fractional cover of different PFTs remains constant, and the biomisation procedure is done once at the start of a model run.

The model determines which biome to consider for each grid cell through a simple Biomisation procedure (Prentice, 1996), and selects one of 8 'fire' biomes (biomes in which fire occur) used. These 8 biomes are based on Pidwirny (2006; original data based on Olson et al, 2001) and are listed in table 1. There is also one 'none-fire' biome (where no fires or predominantly anthropogenic fires occur). The fire model only describes wildfires, so crops fall under 'none-fire' biome. Anthropogenic fires and wildfires in anthropogenic ecosystems could be a source of further study.

	Tropical Savana & season scrub	Tropical & Subtropical Rainforest	Desert	Midlatitude Grassland	Midlatitude Shrubland	Midlatitude deciduous forest	coniferous forest	tundra	No Fire
Tropical BL evergreen tree	0	1	0	0	0	0	0	0	0
Tropical BL deciduous tree	1	1	0	0	0	0	0	0	0
Temperate BL evergreen tree	0	0	0	0	1	0	0	0	0
Temperate BL deciduous tree	0	0	0	0	0	1	0	0	0
Evergreen Coniferous tree	0	0	0	0	0	0	1	0	0
Deciduous coniferous forest	0	0	0	0	0	1	1	0	0
Evergreen Shrub	0	0	1	0	1	0	0	1	0
Deciduous Shrub	0	0	1	1	0	0	0	1	0
C3 Grass	0	0	0	1	1	1	1	0	0
C4 grass	1	0	0	0	0	0	0	0	0
Tubdra Veg	0	0	1	0	0	0	0	2	0
Swamp Veg	0	0	0	0	0	0	0	0	1
Crops	0	0	0	0	0	0	0	0	1

Table 1: Biome matrix. 1 occur when PFT (left) occur in a particular biome (top).

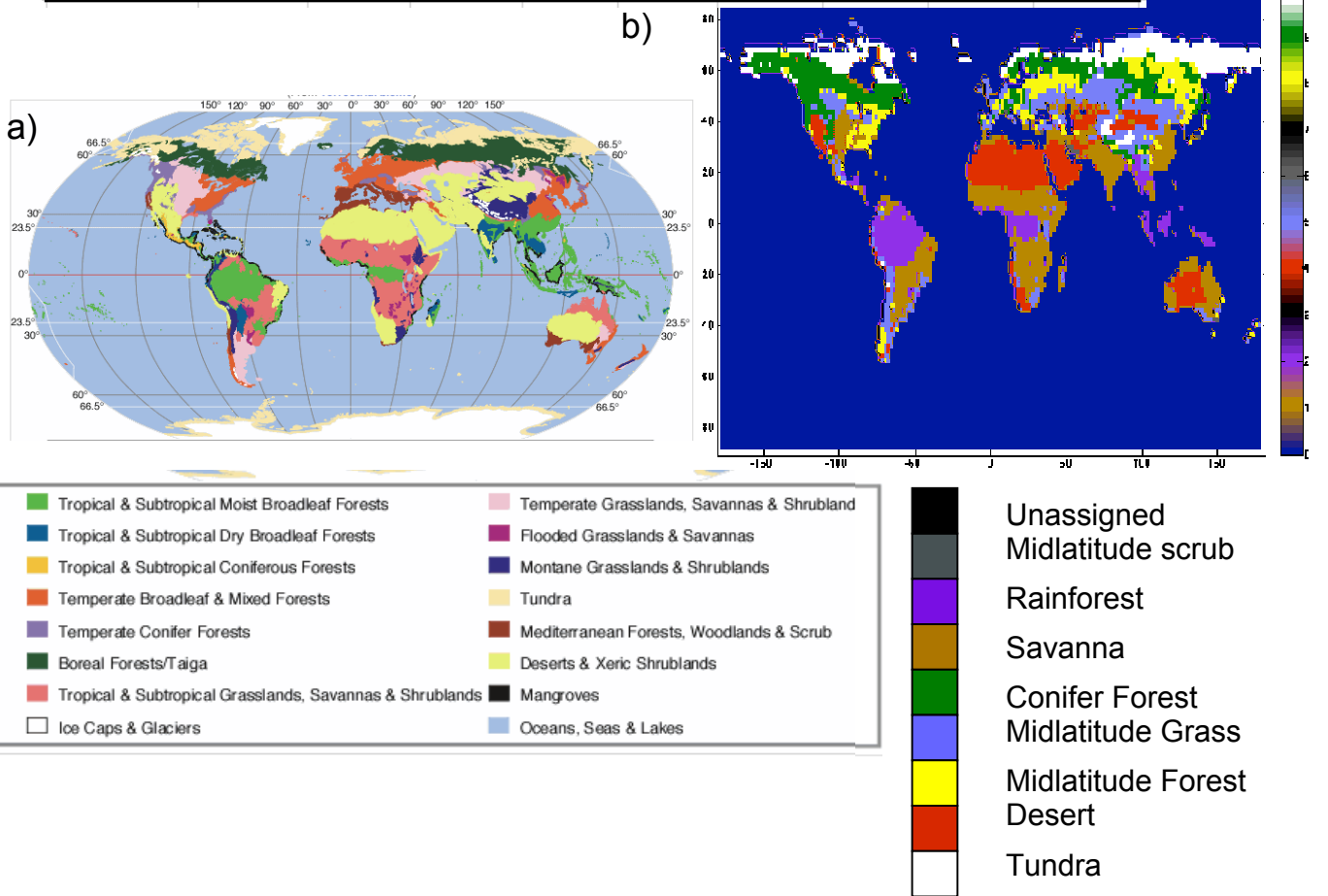


Figure BM2: Global distribution of the Earth's major terrestrial biomes. a)Original Data Source for Map: Olson et al, 2001, taken from encyclopedia of the earth showing 13 major biomes. For this project, Tropical & subtropical Moist Broadleaf Forest and Tropical & subtropical Coniferous forest is referred to as Rainforest, Tropical & subtropical Dry broadleaf Forests and Tropical & subtropical Grasslands, Savannas & scrubland are referred to as Tropical savannah & seasonal scrub., Temperate Conifer forest and Boreal Forest/Taiga are Conifer forests; Temperate Broadleaf & Mixed Forests are Midlatitude/temperate and deciduous forests; Temperate Grassland, Savannas and scrubland are Midlatitude grassland, Flooded Grassland & Savannas and Mangroves (and crops) are no fire, Montane Grasslands and Scrublands are tundra, Mediterranean Forests, woodland and scrub are Midlatitude seasonal scrub and Deserts & Xeric Scrublands are referred to as Deserts. b) Biomes assigned by FISSELING after 1 year spin up in CCDAS for comparison Blue is water; black unassigned, gray Midlatitude scrubland, purple Rainforest; brown, Savanna; green, conifer forest, pale blue, Midlatitude Grassland; yellow, Midlatitude forest; red, desert; white, tundra

To determine the dominant biome, the fraction of each vegetation type is multiplied by the biome matrix (described in table 1 and equation 1). This provides each biome with a score:

$$A_B = \frac{a_B}{\sum_{j=1}^{n_b} a_j} \quad \text{Where } a_B = \sum_{v=1}^{n_v} PFT_{frac,v} \times Bm_{B,v} \quad (1)$$

Where A_j is the affinity score for biome j (affinity score), $Bm_{j,v}$ the value in the biome matrix for biome j and PFT v (table 1), $PFT_{frac,v}$ the fraction of vegetation in the cell covered by PFT v , and n_v the number of different vegetation types for the cell (normally 2 or 3). This is slightly different to standard Biomisation procedures in that the square root of $PFT_{frac,v}$ is not taken. This is to help to distinguish between the fractions of the cell covered by vegetation which experience wildfires from the fraction that doesn't (equation 5). The fraction of the cell, which therefore doesn't experience wildfires, is simply the affinity score for the no fire biome, and is used in further steps. The dominant biome is the fire biome with the highest score, excluding the no fire biome (although the places where they obtain the highest score are shown in figure 3).

Calculations for burnt fraction are done using parameters for this dominant biome on a grid cell level. Burnt fraction is then split between a grid cells corresponding PFT cells, and emissions and mortality are then based on a PFT cell level. Burnt fraction is calculated taking the following steps:

2. Season Length

In the model, season length is driven by fuel load and moisture content of the top soil layer (the litter layer). Previous studies show that, even in favorable climate conditions, fire spread reduces to zero at a threshold fuel. This is due to the fuel bed becoming discontinuous (Schultz, 1988). In FISSLING, if the litter layer of a cell is below this threshold, then burnt fraction is calculated to be zero. If the fuel load is above this threshold, season length in the model is controlled by moisture.

Energy that would otherwise be used in ignition and spread of a fire is first used to evaporate moisture in the litter layer (Viegas, 1997), so the more moist the litter layer is, the less energy there is to propagate the fire. For each day, the probability of a fire occurring is calculated using the following relation (Venevsky et al, 2002), taken from the Nesterov Index (Nesterov, 1949):

$$p(m_d) = e^{-\pi(m_d / m_{e,J})^2} \quad (2)$$

Where $p(m_d)$ is the probability of a fire occurring on a day, d , with litter moisture, and moisture of extinction, $m_{e,J}$ a parameter specific to the dominant biome J . Moisture of extinction is defined as the point at which all available energy is used up vaporizing the moisture, the fuel load does not ignite, and fire only sporadically spreads (Albini, 1976)).

BETHY soil moisture input is on monthly timestep. To estimate the daily fuel moisture content FISSLING calculates daily moisture content through basic linear interpolation (i.e. drawing a straight line) between these monthly values (equation 3) taken to be the moisture half way through the month. Therefore, on the d^{th} day of month j , the moisture content of the fuel load is defined as:

$$m_d = \begin{cases} m_{M-1} + (d + 0.5n_{M+1}) \frac{(m_M - m_{M-1})}{0.5(n_{M-1} + n_M)} & d < 0.5n_M \\ m_M + (d - 0.5n_M) \frac{(m_{M+1} - m_M)}{0.5(n_{M+1} + n_M)} & d > 0.5n_M \end{cases} \quad (3)$$

Where m_M is the moisture content of the month M , containing day d and n_M is the number of days in the corresponding month. As emissions are calculated on a monthly time step, the season length, S , is the sum of the probability of a fire for each day of that month:

$$S = \sum_{d=1}^{n_M} p(m_d) \quad (4)$$

2. Season Length to Burnt Fraction

The dominant fire biome is used to calculate the burnt fraction as follows:

$$B(S) = (1 - A_{nf})S \times e^{f(S)^{-1}C_{J,5}}, \quad f(S) = C_{J,1}S^3 - C_{J,2}S^2 - C_{J,3}S - C_{J,4} \quad (5)$$

Where $C_{J,i}$ are biome specific empirical parameters (table 2) for dominant biome J , derived from satellite data comparison (see below), and A_{nf} is the affinity score for the no fire biome. $C_{J,5}$ takes a value of either 1 or 2. If $C_{J,5} = 2$, then $C_{J,1}$, $C_{J,2}$ & $C_{J,3} = 0$, creating a linear fit (see mid-latitude grassland, mid-latitude deciduous & mixed forest, Desert and Tundra in figure 8). This is because there is lack of accurate data for these biomes. The $(1 - A_{nf})$ term eliminates the proportion of the cell that contains vegetation where wildfire won't propagate from further calculation. This function differs from functions used in previous models such as GLOB FIRM (Thonicke et al, 2001). In these models, burnt fraction is calculated on a yearly time steps, where the exponential function is designed to equal 1 if the season length is the entire year. This assumption does not hold for monthly time steps.

Once burnt fraction has been calculated, it is divided into the PFTs in the cell according to their relative fraction:

$$B_v = PFT_v \times B(S) \quad (6)$$

Where B_v is the burnt fraction for PFT v .

3. Carbon Fire Emissions

The fire model calculates emissions per unit area from the burnt fraction for each PFT within the cell as follows (Seiler & Crutzen, 1980; Hao et al, 1990; Pereira et al, 1999):

$$E_v = FL \times C_{PE,v} \times B_v \quad (7)$$

Where E_v are the emissions for PFT v , FL the grid cell fuel load, and $C_{E,v}$ a PFT specific parameter (emissions or combustion completeness parameter). $C_{E,v}$ is calibrated by CCDAS, arriving at values in table 3. The prior estimate is discussed in section <<>> below.

4. Mortality

Mortality resistant parameters are defined for each PFT, and plant mortality is calculated for each PFT in the cell to be the burnt fraction multiplied by this parameter. Mortality effects the carbon balance (equation 8) and hence fuel load for the next timestep. At this stage, it does not, however, effect the relative vegetation fraction of different PFTs within each cell as the vegetation fraction is set based on real field data, so fire regimes is already factored into PFT composition of each cell. No other processes in BETHY alter the vegetation fraction.

Carbon balance

Adoptions to the carbon balance within BETHY were made to incorporate fire induced plant mortality and carbon emissions from FISSILING. BETHY calculates litter production and loss for each monthly time step for each PFT type in each cell. From production and loss, above ground, living carbon stores and litter layer stores are recalculated. Soil carbon is not explicitly calculated, although litter can be lost to it (see figure 1). Full description of the carbon balance processes can be found at Knorr (1997). Litter production and loss are adapted as follows:

$$\Delta L_+ \rightarrow \Delta L_+ + (FL - \Delta L_+) \eta$$

$$\Delta L_- \rightarrow \Delta L_- - E \tag{8}$$

where ΔL_+ is litter layer production, ΔL_- is litter layer loss, and E or the PFT cell. The left hand side of the equations represents calculations of production and loss without the fire model, the right hand side shows the translation when FISSILING is included.

Litter is lost to either soil carbon or the atmosphere, from which, CO_2 concentrations are simulated (both globally and at points corresponding to CO_2 stations) by TM2 (Heimann, 1995).

3. Data and parameter construction

Satellite Data.

Unlike stand, ground regional burnt data studies, such as the ones used in the construction of glob_firm (Thonicke et al, 2001), long-term observation for active fires made with space born sensors are readily available, capable of producing studies over large areas required for accurate model construction (Giglio et al, 2006). For this reason, parameters for fuel threshold (table 2) and season length to burnt fraction (equation 5) were obtained using Global Fire Emissions Database version 2.1, hereon in referred to as the emissions database (Randerson et al, 2007), and MODIS/Aqua Thermal Anomalies/Fire Daily L3 Global 1km SIN Grid V005, hereon in referred to as thermal anomalies satellite data, as described below:

a. Fuel threshold

To further constrain the threshold value used by the model, monthly satellite data for burnt fraction was compared to satellite data for fuel load over the period of 1997 to 2003 from the emissions database (van der Werf, 2006) For each 1 g/m² of fuel load carbon increase, the maximum burnt fraction for that increase was binned (figure 4). Using a running average, this demonstrates a significant reduction in the maximum

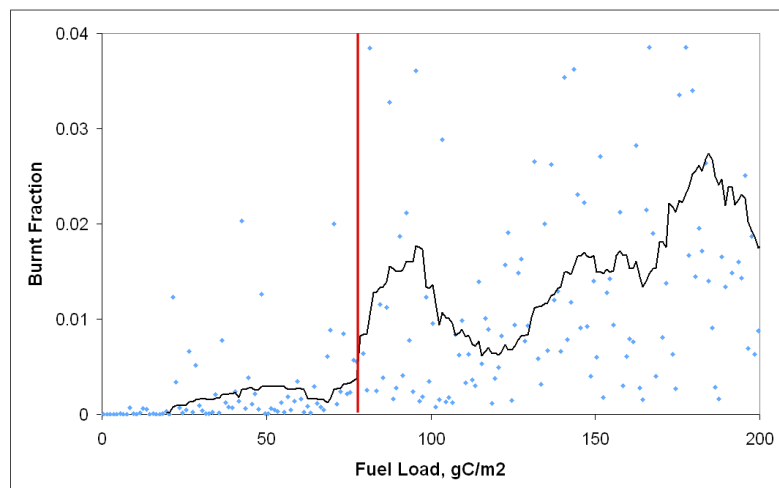


Figure 4: Fuel load vs. maximum burnt area for each 1 gC/m² fuel load increase. Data points are blue dots; black line shows 20 point moving average. Red line shows the point considered to be the fuel load threshold.

burnt fraction at 79 gCm⁻². Schultz (1988) suggests a fuel load threshold of roughly 200 gm⁻² of plant matter. Converting into carbon content, this is roughly the same as the threshold found by Satellite observations (Leeper & Uren 1993).

Biome	$m_{e,j}$ - prior	$m_{e,j}$ - posterior	$C_{j,1}$	$C_{j,2}$	$C_{j,3}$	$C_{j,4}$	$C_{j,5}$	$C_{BE,j}$
Midlat. Scrub	0.2	0.021	0	0	2.972 $\times 10^{-4}$	-0.9268	1	0.04955 \pm 0.02199
Trop. & SubTrop. Rainforest	0.3	0.55	7.537 $\times 10^{-6}$	- 5.251 $\times 10^{-4}$	8.747 $\times 10^{-3}$	-0.1353	1	0.3902 \pm 0.07490
Trop. Savannah	0.25	0.56	- 5.090 $\times 10^{-6}$	1.1385 $\times 10^{-4}$	- 7.156 $\times 10^{-4}$	0.1024	1	0.1639 \pm 0.05498
Coniferous Forest	0.4	0.32	7.537 $\times 10^{-6}$	- 5.251 $\times 10^{-4}$	8.747 $\times 10^{-3}$	-0.1352	1	0.4253 \pm 0.05955
Midlat. Grass	0.12	0.034	0	0	0	-10.66	2	0.08726 \pm 0.06840
Midlat Dec. & mixed Forest	0.25	0.25	0	0	0	-10.11	2	0.4761 \pm 0.07328 6
Desert	0.12	0.077	0	0	0	-9.66	2	0.2881 \pm 0.019 21
Tundra	0.12	0.12	0	0	0	-10.384	2	0.2245 \pm 0.085 81

Table 2: biome parameters for conversion of season length into burnt fraction ($C_{j,1}$ to $C_{j,5}$) and moisture of extinction estimate ($m_{e,j}$). Prior moisture of extinction values were obtained from Burgan et al, 1998 & Thonicke et al, 2001

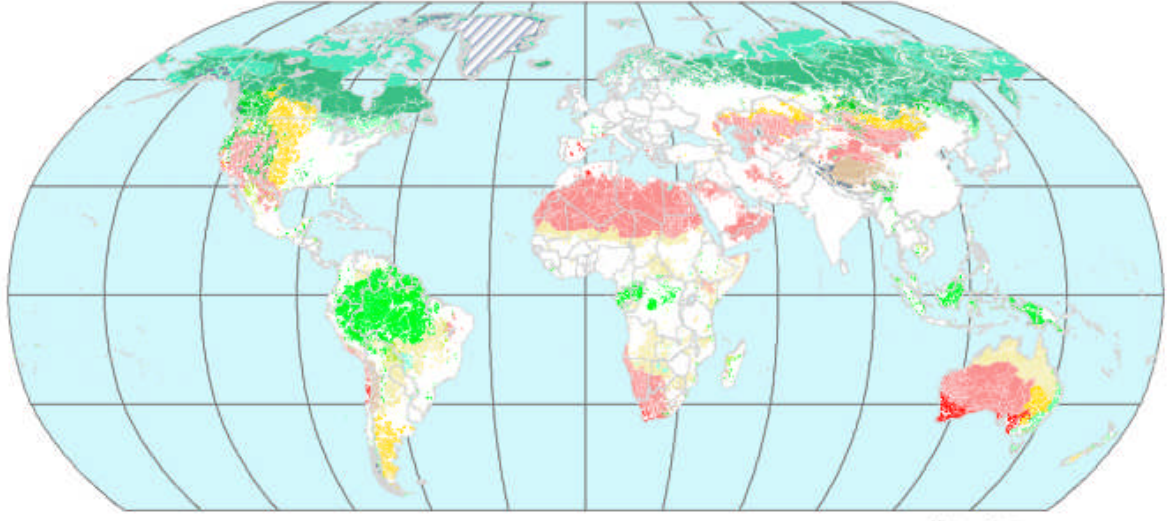
b. Moisture of extinction

Moisture of fuel load is difficult to obtain from Satellite data. Plant moisture can be estimated using Normalized Difference Vegetation Index (NDVI; Burgan and Hartford, 1996), however, NDVI is a measure of plant greenness (and thus a measure of planet health) and only shows correlation to litter layer moisture (the source of ignitions) for a few vegetation types that only obtain moisture from the upper soil layer. Otherwise, there is an indeterminate time lag between plant and litter layer moisture content (Chuvieco et al, 2004). Normalized Difference Water Index (NDWI; Sims & Gamon, 2003) has also been developed, using bands at 850 and 1200nm instead. This has shown considerable improvement on NDVI as a predictor of fuel moisture (Dennison, 2005). This has only been used for regional studies so far, and no global dataset exists. Production of a global dataset may help the development of models such as this, as well as regional fire forecast models.

In this model, prior moisture of extinction was based on field studies (values and references in table 4). FISSLING was run uncoupled from CCDAS and driven by input data used in BETHY for PFT type and fraction and cell moisture content. The simulated burnt fraction was optimized against 1997 to 1999 burnt fraction taken from the emissions database for specially selected study regions with a HPI of less the 0.1 (figure 5; Last of the Wild version 2, 2005) in an attempt to exclude anthropogenic fires. This was done by minimizing the following cost function:

PFT	$C_{PE,N}$ prior	$C_{PE,N}$ prior uncertainty	$C_{PE,N}$ posterior	Mortality
Trp. BL evergreen tree	0.087	0.068	0.1950	0.5
Trp. BL deciduous tree	0.282	0.071	0.1422	0.5
Temperate. BL evergreen tree	0.425	0.060	0.4250	0.5
Temperate. BL deciduous tree	0.164	0.055	0.1641	0.12
Evergreen coniferous tree	0.390	0.075	0.3901	0.12
Deciduous coniferous tree	0.315	0.069	0.3256	0.12
Evergreen Shrub	0.402	0.038	0.3936	0.5
Deciduous Shrub	0.335	0.052	0.3350	0.5
C3 Grass	0.271	0.068	0.3419	0.88
C4 Grass	0.476	0.073	1.049	0.88
Tundra Veg	0.356	0.02	0.3560	1
Swamp Veg	0.5	0.5	0.4999	1
Crops	0.5	0.5	0.4059	1

Tables 3, parameters for individual PFTs. 1st two columns show prior estimates and uncertainties for the optimized parameters for carbon emission. Column 3 shows the optimized emission parameters, and the final column shows the value used for mortality, taken from Thonicke et al, 2001; Mark et al, 2003; Cochrane & Schulze, 1999; Haugaasen, 2000; Holdsworth & Uhl, 1997.



Last of the Wild

Figure 5: Taken from SANDERSON et al. Last of the Wild, showing biomes with a human footprint index of less than 0.1. Colour on map correspond to Biome key



$$\varphi = \sqrt{\sum_g^{n_g} (B_{obs} - B_{sim, m_e})} \quad (10)$$

This simple optimization, similar to Stage 1 optimization already employed by CCDAS, (figure 1), is possible as burnt fraction per cell within the model does not interact with neighbouring cells, and therefore each moisture of extinction is an independent variable. Values obtained for moisture of extinctions are given in table 3.

c. Burnt fraction vs. thermal anomaly

The coefficients in equation 5 for conversion of season length to burnt fraction were determined by comparing season length calculated from Modis thermal anomalies satellite data with burnt fraction data from the emissions database. This was done on a series of study regions for the period of 2003 to 2005. Each study region was a size of 2 by 2 degrees, The 2 by 2 degree size was selected as it is small enough to capture season length of an area for just one biome all within the same season (i.e., it wont have a summer fire season in one part of the region, whilst having monsoonal effects in another), whilst being broad enough to get a large amount of sampled thermal anomalies

pixels (approximately 20000 to 50000, depending on the latitude). At least two study regions were picked for each biome, except multitude grassland, for reasons discussed below (figure 6 and table 4), and each biome contains at least 10 data points (i.e. at last a total of 10 months with a measurable fire season and burnt area) from all study regions. No study region represents more then 2/3rds of the total data points for the biome, except again for multitude grassland. regions were selected so as to match the following critical, based in importance order

1. At least one month with a measurable fire season and burnt fraction
2. Minimum possible Human Footprint Index (HPI; Sanderson et al, 2002)

Thermal anomalies dataset was used to determine the monthly season length through the detection of hot spots of high surface temperature, with consistent monitoring of burning

patterns at high temporal resolution (Cahoon *et al.*, 1992; Justice & Dowty, 1994; Nelson, 1994; Barbosa *et al.*, 1999; Dwyer *et al.*, 2000) based on thermal emission responses of fires in the middle infrared and thermal inferred bands (using the algorithm in Giglio *et al.*, 2003. Before this could be done, the dataset needed georeferencing and *matching* to the *region*. Modis Thermal Anomalies Data was provided in datasets of 1200 by 1200, 1km pixels, with the longitude and latitude of each corner of the dataset provided. The range of each thermal anomalies dataset was

Table 4: Study regions with position, assigned biome, data point and total burnt fraction over the 3 year study period

Study Region	Longitude	Latitude	Biome	Data points	Total BF
MS1	128	-14	Midlatitude Scrubland	33	2.595E-02
MS2	-107	26	Midlatitude Scrubland	16	6.255E-03
TR1	14	4	Tropical Rainforest	24	4.673E-03
TR2	49	-14	Tropical Rainforest	21	1.375E-02
TR3	-78	0	Tropical Rainforest	23	4.376E-03
TR4	-60	-8	Tropical Rainforest	19	0.1151
TR5	146	-36	Tropical Rainforest	31	0.1946
TR6	109	32	Tropical Rainforest	4	2.487E-05
TS1	140	-36	Tropical Savana	30	9.907E-03
TS2	-8	16	Tropical Savana	27	0.1632
TS3	-68	-36	Tropical Savana	21	9.618E-03
TS4	80	20	Tropical Savana	27	7.187E-02
CF1	46	60	Conifer Forest	4	9.159E-04
CF2	136	58	Conifer Forest	3	2.186E-03
CF3	110	56	Conifer Forest	14	7.513E-02
MG1	-3	38	Midlatitude Grassland	20	2.541E-03
MD1	-80	39	Midlatitude deciduous Forest	29	4.212E-03
MD2	109	34	Midlatitude Deciduous Forest	4	1.254E-04
DS1	16	-24	Desert	4	4.291E-03
DS2	-104	26	Desert	14	2.000E-03
TU1	-126	59	Tundra	6	2.336E-03
TU2	38	68	Tundra	1	7.346E-05
TU3	50	68	Tundra	1	1.021E-04
TU4	40	68	Tundra	1	1.224E-04
TU5	-128	59	Tundra	5	7.444E-04

between 10deg, 50" and 42deg and 30" of longitude, depending on the latitude, and 10deg 50" and 7deg 30" depending on the angle the swath make with the elliptic. Emissions database provided information on global burnt fraction on a 1 by 1 deg resolution, and study regions were 2 by 2 degrees. To match up the two datasets, the thermal anomalies data needed georeferencing by:

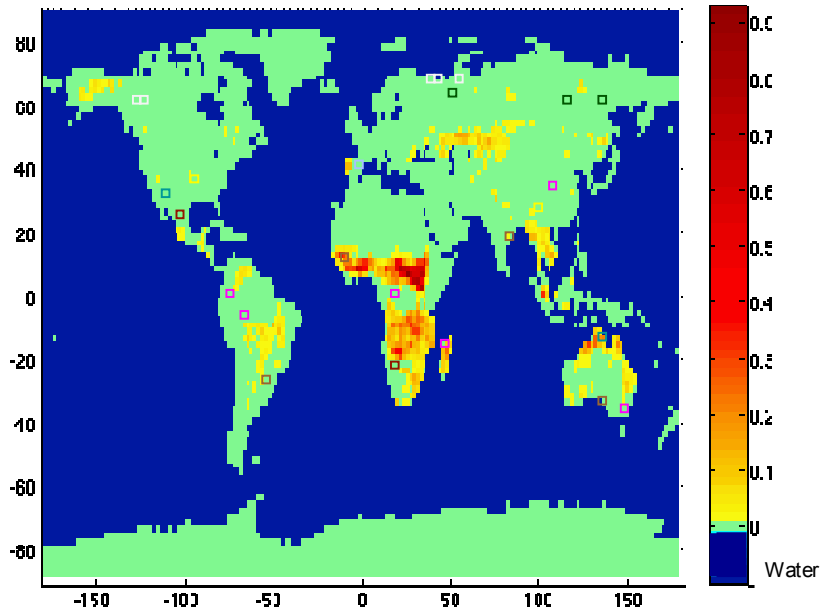


Figure: 6, global burnt fraction taken from fire emission database. Scale on left is average burnt fraction over the three study years, 2003-2005. Squares represent study regions: Blue is midlatitude scrubland; purple, Tropical and Subtropical broadleaf rainforest; light brown, tropical savannah and tropical seasonal & scrub; green, conifer forest; lilac, multitude grassland; yellow, midlatitude deciduous; red, desert and white, tundra.

1. 'Flip' and 'Rotate' the data image to line up the images corners to the correct coordinated (Barrett & Leonard, 1999)

$$\begin{aligned}
 TA_{i,k} &\rightarrow TA_{n_{px}-k+1,i} && \text{(Rotate)} \\
 TA_{i,k} &\rightarrow TA_{i,n_{px}-k+1} && \text{(Flip)} \\
 TA_{i,k} &\rightarrow TA_{n_{px}-k+1,n_{px}-i+1} && \text{(Overall)} \quad (11)
 \end{aligned}$$

Where $TA_{i,k}$ is the thermal anomalies data for pixel i,k in the image and n_{px} is image height/width in pixels (swadth width)

2. Georeference each pixel with the following steps:
 - a) Using equations 12 (Nair & Staniforth, 1999), find the position of pixel $TA_{i,k}$, where λ_1 & ϕ_1 and λ_2 & ϕ_2 is the latitude and longitude of the top left & tope right corners of the image respectively, and, in this case, $\lambda_{i,k}$ and $\phi_{i,k}$ is the

latitude and longitude of pixel $TA_{i,1}$ (i.e., $k=1$) and $fr = \frac{i}{n_{px}}$ is the fractional

distance between the two points

b) Find the position of $TA_{i,n_{px}}$ (latitude $\lambda_{i,k}$ and longitude $\phi_{i,k}$), this time with λ_1 & ϕ_1 and λ_2 & ϕ_2 representing latitude and longitude of the bottom left and right corners, and again, $fr = \frac{i}{n_{px}}$.

c) Find position $TA_{i,k}$ where λ_1 & ϕ_1 is longitude and latitude calculated in part a) for $TA_{i,1}$, λ_2 & ϕ_2 in part b) for $TA_{i,n_{px}}$, and $\lambda_{i,k}$ and $\phi_{i,k}$ the position of

$TA_{i,k}$. This time, $fr = \frac{j}{n_{px}}$

$$D_1 = 2 \sin^{-1} \left(\sqrt{\frac{\sin^2(\lambda_2 - \lambda_1)}{2} + \cos(\lambda_1) \cos(\lambda_2) \sin^2(\phi_2 - \phi_1)} \right)$$

$$D_2 = \frac{\sin(D_1(1 - fr))}{\sin(D_1)}$$

$$D_3 = \frac{\sin(D_1 \times fr)}{\sin(D_1)}$$

$$X = D_1 \cos(\lambda_1) \cos(\phi_1) + D_2 \cos(\lambda_2) \cos(\phi_2)$$

$$Y = D_1 \cos(\lambda_1) \sin(\phi_1) + D_2 \cos(\lambda_2) \sin(\phi_2)$$

$$Z = D_1 \sin(\lambda_1) + D_2 \sin(\lambda_2)$$

$$\lambda_{i,k} = \begin{cases} \frac{\pi}{2} \operatorname{sgn}(Z) & X, Y = 0 \\ a \tan\left(\frac{Z}{\sqrt{X^2 + Y^2}}\right) & \text{else} \end{cases}$$

$$\phi_{i,k} = \begin{cases} \tan^{-1}(Y/X) & X > 0 \\ \frac{\pi}{2} \operatorname{sgn}(Y) & X = 0 \\ \tan^{-1}(Y/x) + \pi \operatorname{sgn}(Y) & X < 0 \end{cases} \quad (12)$$

- Exclude cells from thermal anomalies dataset that are outside the study region by: excluding pixels with a latitude greater then the latitude band representing the top of study region, and less then the band representing the bottom; and excluding pixels with a longitude less then the left hand longitudinal band, and greater then the right.

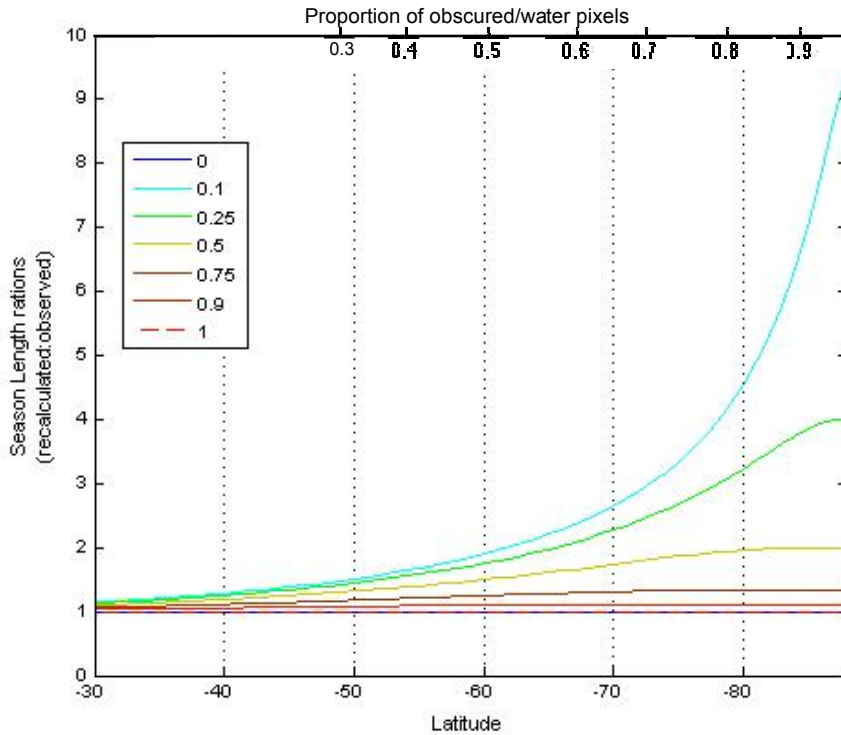


Figure 7: Manipulation of observed season length according to different longitudes / different obscured and water pixels. Light blue; for a season length of: blue, 0.1 month; green, 0.25 months; yellow, 1/2 month; brown, 0.75 months; red, 0.9 months. 1 Months (red dashed) and 0 month (purple dash) remains unchanged.

Once all but the study region was excluded, the season length for each month was calculated by finding the amount of days within that month where there was at least one pixel in the thermal anomalies data set with either nominal or high confidence fire occurrence. As the study regions were 2 by 2 degrees, regions at high latitude covered smaller area. Also, water and obscured pixels (i.e. by cloud or dust storms etc) made the area sampled within the region vary. To correct for this equation 14

was used to convert the observed season length to the season length expected for an equatorial 2 by 2 degree cell (figure 7) , composed entirely of un-obscured land pixels.

$$S = n \left(1 - \left(1 - \frac{S_o}{n_M} \right)^{1/R} \right) \quad \text{with} \quad R = \frac{\sin(\lambda_a) - \sin(\lambda_b)}{\sin(\Delta\lambda_{rg})} \left(1 - \frac{P_h}{P_T} \right) \quad (14)$$

where S is the converted season length used for the rest of this parameter selection, S_o is the observed season length, n_M is the number of days in the month and R is the ratio the total number of unhidden land pixels in the study region over the month to the total amount found in the perfect equatorial study region. The first part of function R describes alterations made for different latitudes, with λ_a and λ_b being the latitude boundaries of the study region, and $\Delta\lambda_{rg}$ the difference in latitude of the study regions (in this study, two degrees), P_h the number of hidden or water pixels, and P_T the total amount of pixels in the study region (i.e. number of none-excluded pixels in part 3 of georeferencing).

The burnt fraction for the study regions was calculated using the 4 data points in the global burnt fraction from the emissions database. In this database, which is 1 deg by 1 deg resolution, burnt fraction is calculated from a variety of different remote sensing sources, using the procedure described in Giglio et al, 2006. Briefly, are burned is proportional to counts of fire pixels in a remote sensing image contained within the 1deg cell:

$$B(\underline{x}, t) = \alpha N_{fpx}(\underline{x}, t) \quad (15)$$

where $B(\underline{x}, t)$ is the burnt fraction over the spatial region \underline{x} and time period t , $N_{fpx}(\underline{x}, t)$ is the number of fire pixels observed, and α is a conversion factor. This database differs from different burnt fraction products in that α varies with tree herbaceous vegetation cover, fire pixel cluster size and de-forestation extent. This last factor makes the database particularly useful as it allowed for correction in anthropogenically diminished study area within the study regions.

Each data point was weighted depending on the area it represented relative to every other point using:

$$B = \frac{(B_{\lambda_a, \phi_f} + B_{\lambda_a, \phi_g})(\sin(\lambda_a) - \sin(\lambda_c)) + (B_{\lambda_c, \phi_g} + B_{\lambda_c, \phi_f})(\sin(\lambda_c) - \sin(\lambda_b))}{\sin(\lambda_a) - \sin(\lambda_b)} \quad (16)$$

The converted season length was compared to calculated burnt fraction data to calibrate the coefficients in equation 5 (figure 8 and table 2) using least square fitting with the additional condition

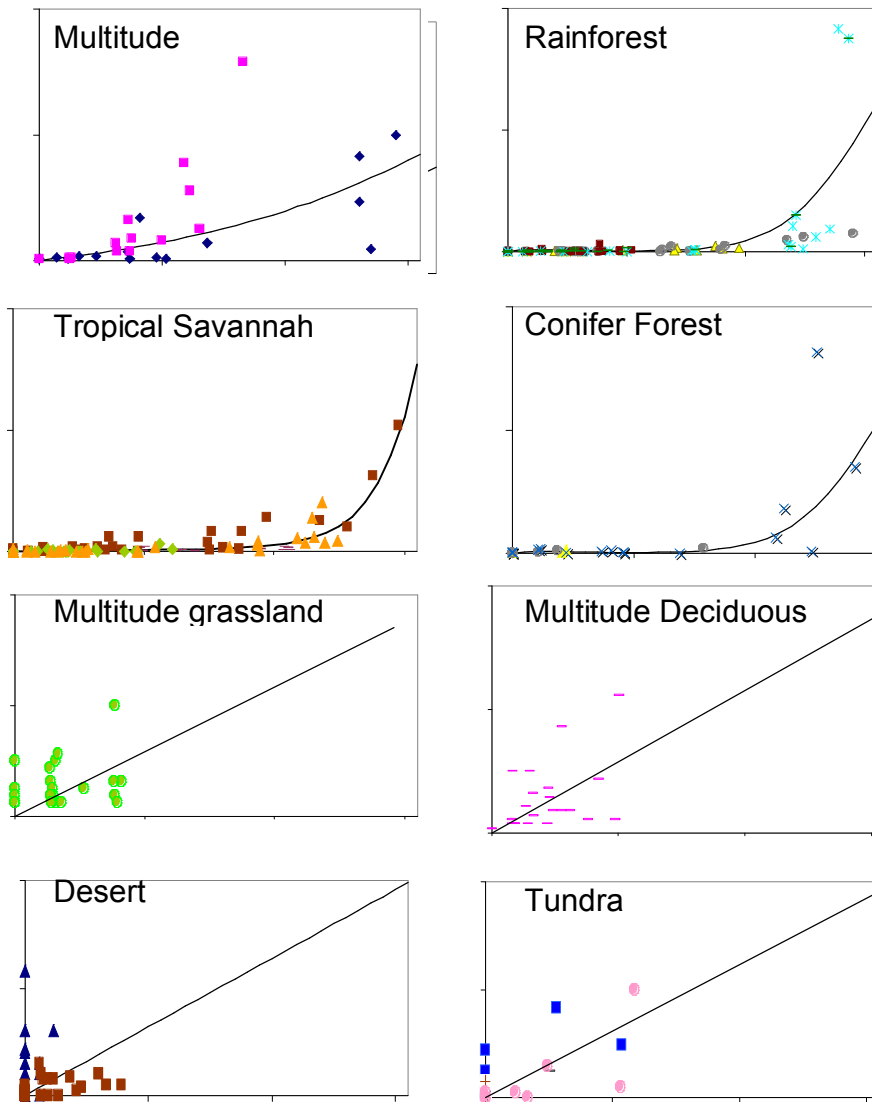
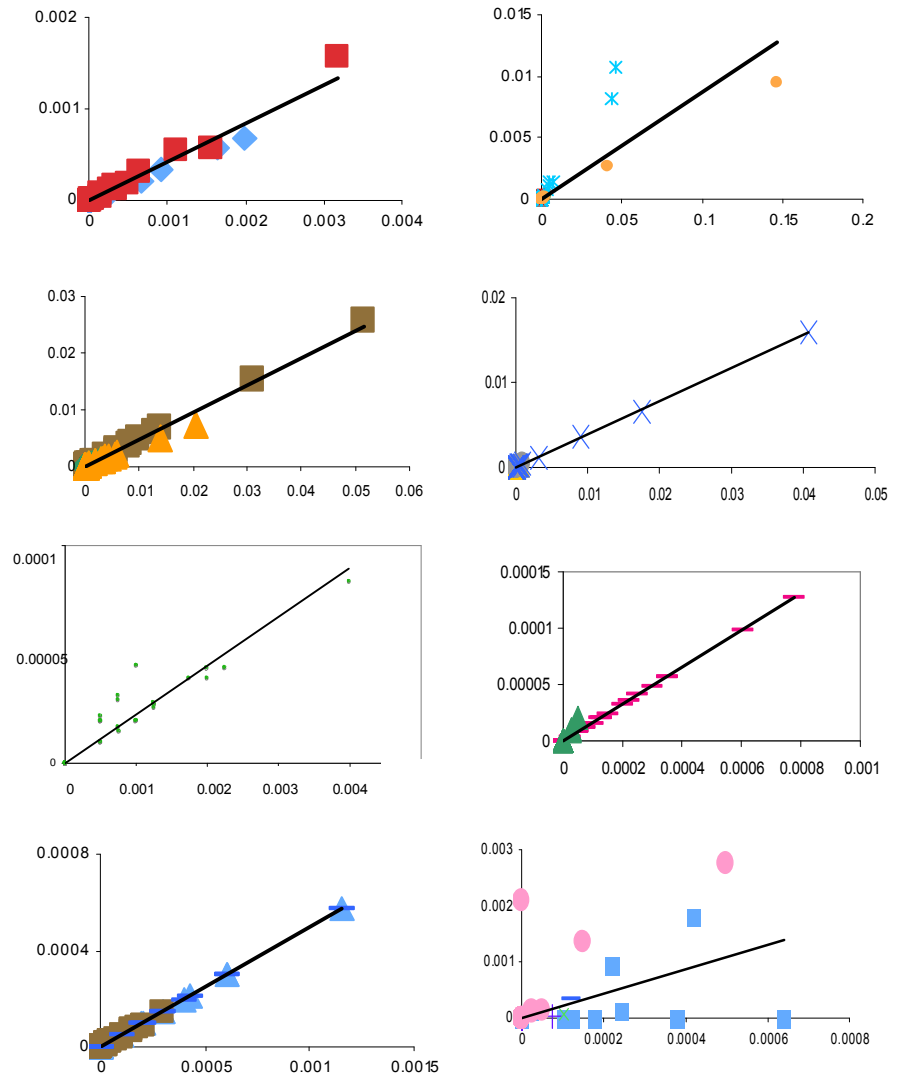


Figure 8: Burnt fraction vs. corrected season length. Equation 5 Was used in full for trendline in a) mid-latitude scrubland b) tropical and subtropical rainforest, c) tropical savannah and seasonal scrub and d) conifer forest. Parameters A,B & C were zero in e) mid-latitude grassland, f) mid-latitude deciduous forest, g) desert and h) tundra. Data points correspond to regions in Table D2.1 as follows: a) diamonds, MS1; squares, MS2; b) triangles TR1; circles, TR2; squares, TR3; stars, TR3; dashes, TR5; c) dashes, TS1; squares, TS2; diamonds, TS3; triangles, TS4; d) triangles, CF1; circles, CF2; crosses, CF3; e) circles, MG1; f) dashes, MD1; g) triangles, DS1; squares, DS2; h) squares, TU1; cross, TU2; dash, TU3; star, TU4; circle, TU5

that the function must have a positive gradient for season lengths from zero to an 31 days (i.e. longer season length within a month always means a higher burnt fraction), and that after 31days the function must be less then 1.

The nature of the burnt fraction from emissions database meant that months with very low burnt fractions were less well constrained then ones with high burnt fraction (Giglio et al, 2006). Because of this data sets for 4 of the 8 biomes (multitude grass and deciduous and mixed forest, Desert and Tundra) had $C_{j,i}$ ($i \in [1,3]$) and $C_{j,i} = 2$ in equation 5 were set to zero and. This produces a linear fit (see figure 8). A possible step forward with the model would be to reconstruct these data sets

Figure 9: Burnt fraction vs. Combustion Completeness with linear fit trendline in a) mid-latitude scrubland b) tropical and subtropical rainforest, c) tropical savannah and seasonal scrub and d) conifer forest. Parameters A,B & C were zero in e) mid-latitude grassland, f) mid-latitude deciduous forest, g) desert and h) tundra. Data points correspond to regions in Table D2.1 as follows: a) diamonds, MS1; squares, MS2; b) triangles TR1; circles, TR2; squares, TR3; stars, TR3; dashes, TR5; c) dashes, TS1; squares, TS2; diamonds, TS3; triangles, TS4; d) triangles, CF1; circles, CF2; crosses, CF3; e) circles, MG1; f) dashes, MD1; g) triangles, DS1; squares, DS2; h) squares, TU1; cross, TU2; dash, TU3; star, TU4; circle, TU5



with either more accurate satellite data processing algorithm for small burnt fractions or by using detailed field studies. The relative contribution to emissions on the biomes is likely to be relatively small, with the exception of burning of aggregate forest slash in mid-latitude deciduous and mixed forests (Giglio et al, 2006).

d. Emission parameters

Emission parameters were calibrated in CCDAS. These parameters require a prior value and uncertainty. This was done by using combustion completeness dataset from the emissions database. In the database, combustion completeness is calculated through variations in global NDVI (Werf et al, 2006), combined with field study measurements. Combustion Completeness is

treated as a function of: fuel type (when fuels have had more time to dry; Hoffa et al, 1999) period in fire season; and fuel dryness (Hoffa et al; 1999). Most biomes seem to be reasonably portrayed by the database, with the exception of tropical biomes (van der Werf, 2006).

The combustion completeness for each study region & month was calculated in the same way as burnt fraction in equation 16. The fuel load that is converted into co2 emissions is taken as the combustion completeness multiplied by the fuel load. For each biome, the emissions parameter and uncertainty was taken to be the coefficient of the linear best fit and root of the variance respectively (figure 9)

To obtain prior estimates for emission parameters and uncertainty on these parameters for individual PFTs, a 'reverse Biomisation' procedure was developed. The procedure adds the biomes emission parameter for each biome the PFT is found in, and divides it by the number of biomes containing that PFT:

$$C_{PE,v} = \frac{\sum_{j=1}^{n_b} C_{BE,j} \times Bm_{j,i}}{\sum_{j=1}^{n_b} Bm_{j,i}} \quad (17)$$

Where $C_{BE,j}$ are the emissions parameter for biome j, and n_b the number of biomes. Uncertainties were calculated using squares:

$$\sigma_{PE,i} = \sqrt{\frac{\sum_{j=1}^{n_b} (\sigma_{BE,j})^2 \times Bm_{j,i}}{\sum_{j=1}^{n_b} Bm_{j,i}}} \quad (18)$$

Where $\sigma_{PE,i}$ is the prior estimate for the uncertainty of $C_{PE,v}$ and $\sigma_{BE,j}$ is the root of the variance when obtaining $C_{BE,j}$

e. Mortality

Mortality is also tricky to obtain from satellite data, due to the different rates of post-fire mortality and difficulties in assigning the causes of mortality between fire and other process, often occurring

hand in hand with fire (such as draught; Mark et al, 2004). Previous field studies have therefore also been used to obtain mortality parameters (table 4). In the future, it may be useful to optimized mortality parameters in CCDAS. This, however, is beyond the scope if this study.

4. Model Validation and Evaluation

The parameters were optimized in step 2 CCDAS over the period of 1979 to 1999 on a low resolution.

Observational satellite data is available from emission database for 1997. Over the period of study, the average model output monthly fast respiration carbon emissions

1.66 PgC , or 19.9 $PgC yr^{-1}$, while fire emissions were

0.018 $PgC mnth^{-1}$ or 0.22 $PgC yr^{-1}$. van der Werf et al (2006) estimated a value of 58 $PgC yr^{-1}$ & 2.5 $PgC yr^{-1}$ for heterotrophic respiration and fire emissions respectively over the years 1997-2004. Both the results from the model are considerably different to observations. However, the ratio of fire emissions to respiration emissions from the model over the El Nino years of 97-99 is around 2%, close to the reported value of 4% by van der Werf et al (2006). Also, for the period 1997 to 1999, the timing of larger fire emissions correlates from both emissions database and the model shown in figure 10. Figure 10 also show average monthly climate data for precipitation for the Amazon rainforest. This is calculated from historical weather data (GHCN-Monthly). The monthly average was taken by averaging the historical data over all station which fall inside the Amazon Nino study region using:

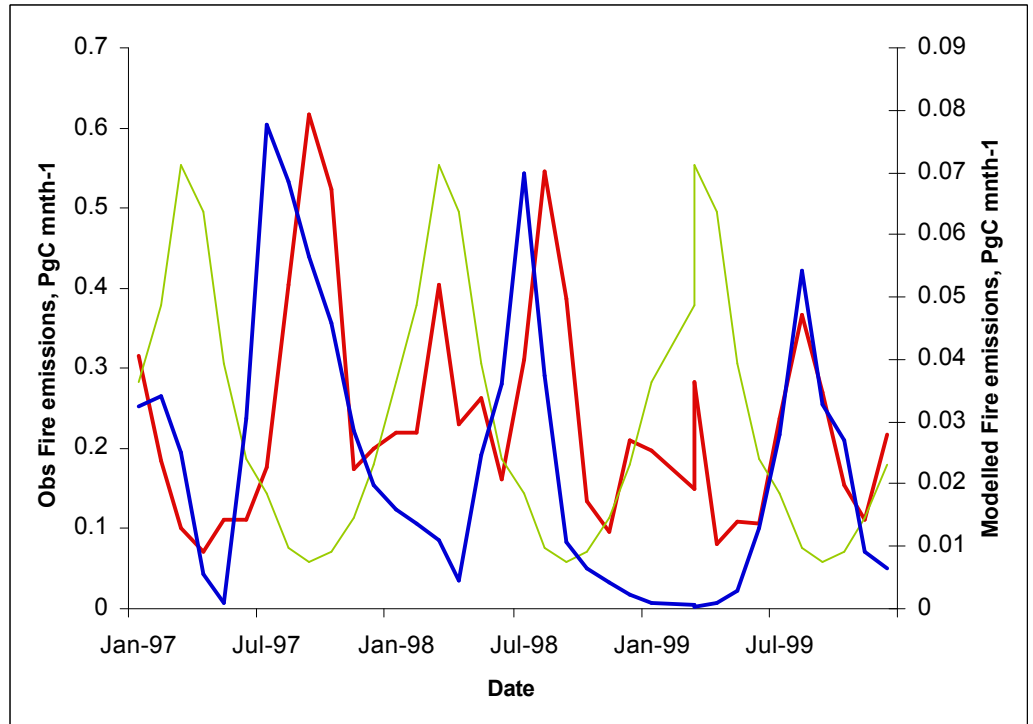


Figure 10: Fire Carbon emissions from emissions database (red, right hand axis) vs. those simulated by the model (blue, left hand axis) for the Amazonian emissions study region. Green line shows variability in precipitation in the Amazonian region.

$$W = \frac{\sum_{i=1}^{n_{Stw}} (St_i \times n_{Sty_i})}{n_{Stw} \sum_{i=1}^{n_{Stw}} n_{Sty_i}} \quad (19)$$

Where W is the precipitation for a particular month, St_i the historical precipitation & n_{Sty_i} is the number of years the historical data is based upon for weather station i , and n_{Stw} is the number of weather stations. Precipitation in the rainforest is a good proxy for fuel moisture. Therefore, when precipitation is high (January through to May), fuel moisture content will be high. It is at these times that the model no longer correlates quantitatively with emissions database observations. This could be due to problems with the interpolation process used to determine daily fuel load moisture (equation 3), as it assumes a uniform change in moisture availability, whereas in reality, due to periods of high precipitation or heat, fuel load moisture may be a lot more variable. This could cause daily transitions of moisture across the moisture of extinction threshold, which would not show on the linear interpolation used in this model, and would specially screw simulations when moisture values are close to the moisture of extinction. The result would be a reduced fire occurrence and emissions seen in the model output for these periods of high moisture.

During the times of these large emissions, both fire emissions and respiration are one order of magnitude less than reported by van der Werf (2006). These reduced emissions may be a result of a combination of several factors including:

- Local minima in the gradient during optimization. The optimization process may have found a point in the parameter space such that for any movement around this point would result in an increase in the value of the cost function. This may be a problem with inaccurate prior estimates and uncertainties on the input parameters
- Problems associated with the lack of detailed carbon emissions (both fire and respiration) due to the low resolution of the optimization. This is currently being explored further through conducting a high-resolution optimization, not possible in the time frame of the project.
- Problems in the model itself, including the interpolation between moisture data points already discussed, and inaccuracies in parameters such as the ones describing the conversion of season length to burnt fraction (equation 5). More data points could be collected for equation 5 to try and resolve this. Problem with moisture interpolation would require more exploring. The model does not consider anthropogenic fires either. Although this wouldn't effect the models simulated emissions normally by an order of magnitude, it

may create additional local minima's for the optimization process to get stuck in. No plans for developing an anthropogenic ignition source have been developed at the moment, but models such as SPITFire (again, an LPJ fire model, this time entirely process driven; Thonicke et al, unpublished) do include this already.

To explore accuracy of intermediate steps, assigned biomes (figure 3) and average yearly burnt fraction for the period 1997-2003 (figure 11) are displayed against observation from Pidwirny et al (2006) Biome map and emissions database burnt fraction respectively. The biomes are from a high resolution run, decoupled from CCDAS, whereas burnt fraction is one a low resolution produced after optimization. The model seems to qualitatively simulate the burnt fraction of most regions well, with the exception of Australia, where Western Australia has an anonymously high-simulated burnt fraction. This seems to be down to a problem in biome allocation (figure 3), with biomisation predicting savanna instead of mid-latitude season and scrubland.

For a more through analysis of the accuracy of simulation of burnt area, high resolution optimization would be required (discussed above), as at the moment, observational grid cells do not correspond to simulated cell, and not all land (e.g. Indonesia) is defined in low resolution.

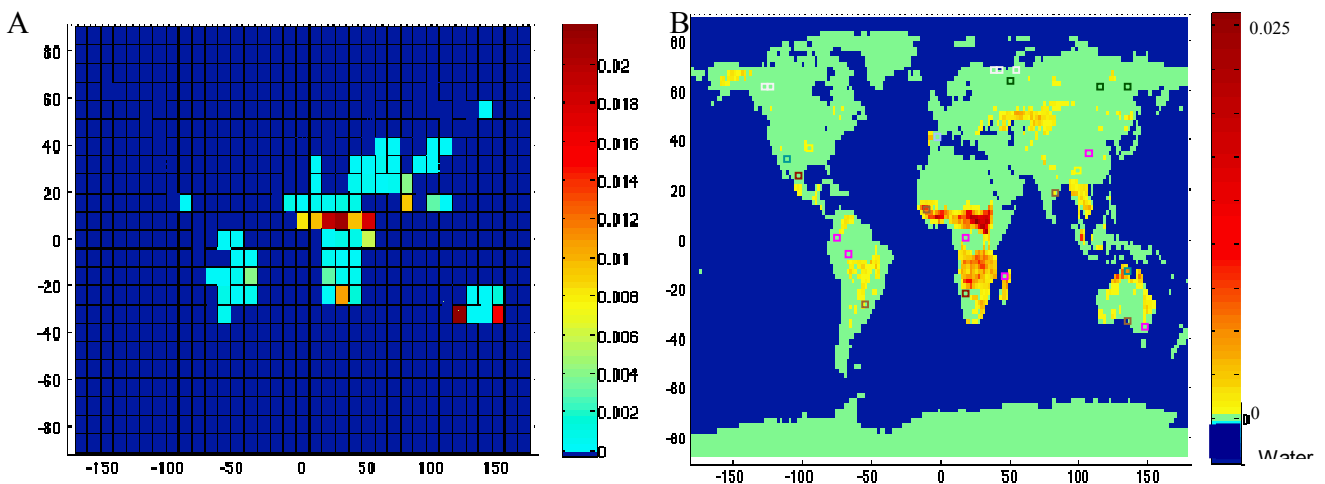


Figure 11: a) Simulated burnt fraction on a low-resolution grid, b) converted from emissions database to a 2deg grid. Colour bars indicate burnt fraction.

5. Results

ENSO

To explore the effects of ENSO on fire emission, and the resulting contributions to the variation in interannual CO₂ concentrations, global total fire emissions (figure RE1), and emissions from 2 Niño study regions, over the Amazon (± 10 deg lat, -45 to -65deg lon) and Indonesian (± 10 deg lat 95 to 155 lon) Rainforests, were calculated on a month by month basis from emission database satellite data for 1997-2003 (figure 12). As the resolution of the model was too coarse to include Indonesia, the simulated emissions from couple BETHY and FISSLING was calculated for global and Amazonian regions only (figures 13 onwards) for the period of 1979 to 1999. Global contributions from terrestrial respiration were also calculated (figure RE1) for the Amazon and globally for 1979-1999.

These were compared to the Oceanic Niño Index (ONI), which is defined as the three month running average sea surface temperature contrast between eastern and western Pacific in the Niño 3.4 region (5°N-5°S, 120°-170°W; Smith and Reynolds, 2003). Events are defined as 5 consecutive months with at least +0.5° (El Niño) or at least -0.5 anomaly (La Niña). These are further broken down into Weak (with a 0.5 to 0.9 SST anomaly), Moderate (1.0 to 1.4) and Strong (≥ 1.5) events.

During the study period, El Niño events have occurred during: 1982-1983; 1986-1987; 1991-1992; 1993; 1994; 1997-1998; 2002-2003; 2004-2005 and 2006-2007 (IPCC, 2007), with 1982-1983 and 1997-1998 being unusually large (Rasmusson, 1985; Trenberth 2002). The major El Niño events of 1997-1998 brought the phenomenon to worldwide attention and temporarily warmed air temperature by 1.7°C over the Eastern Pacific compared to the usual increase of 0.3°C associated with most events (Trenberth 2002). Over the study period, La Niña events occurred in: 1988-1989; 1995; 1999-2000. The 1988-1989 event, as well as the event occurring now (starting in 2007, outside the study period) are particularly strong.

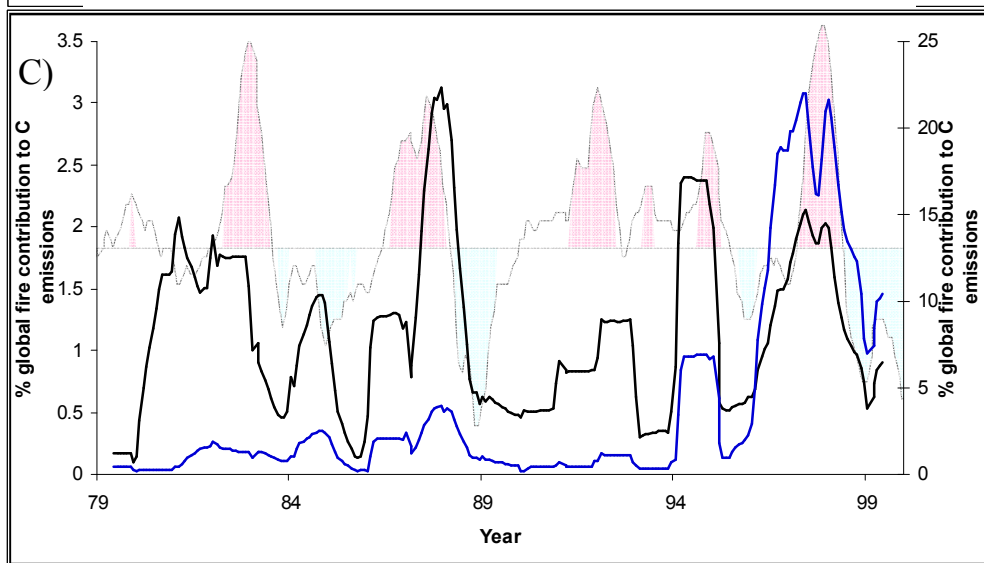
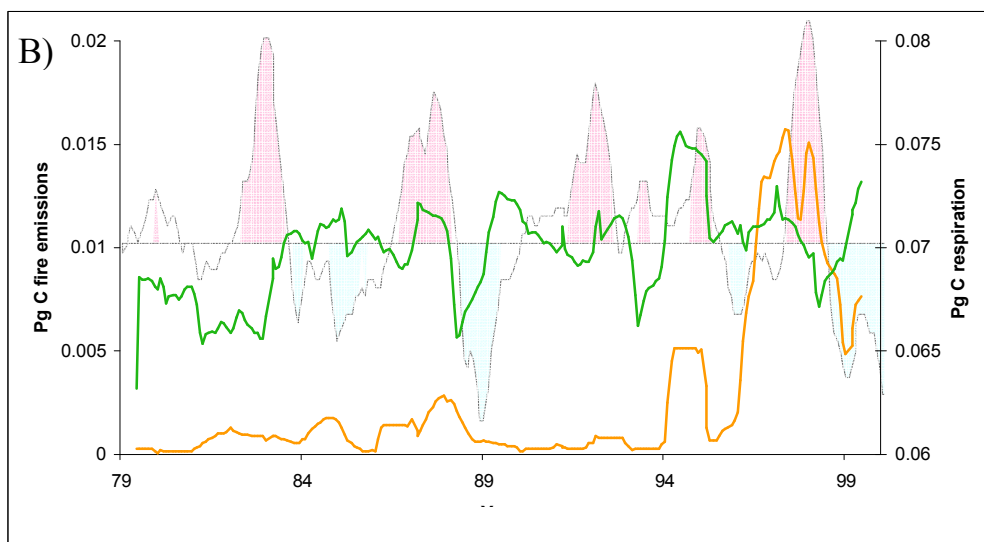
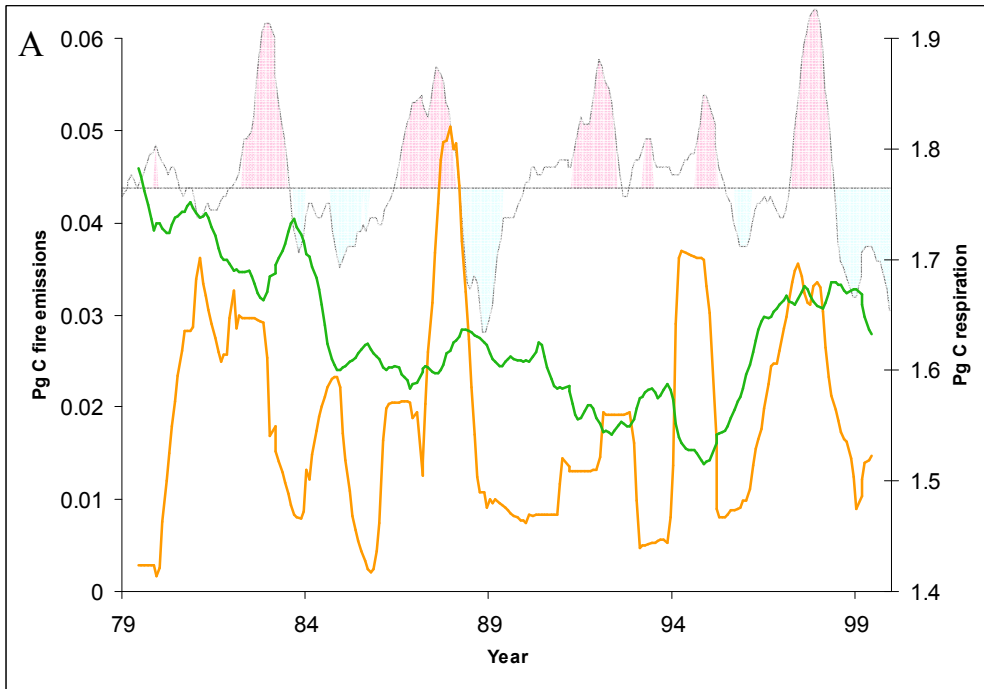


Figure 13: a) % of fire emission contribution compared to total fire carbon and respiration carbon emissions for (black, left hand side) global and (blue, right hand side) Amazon Nino regional, b) global and c) Amazon Nino region carbon emission from respiration (green) and fire (orange) modeled by the couple FISSLING and BETHY model after optimization through CCDAS during the study period of 1979 to 1999. Watermarked lines in background show ONI. Red shaded is El Nino and blue shaded in La Niña conditions.

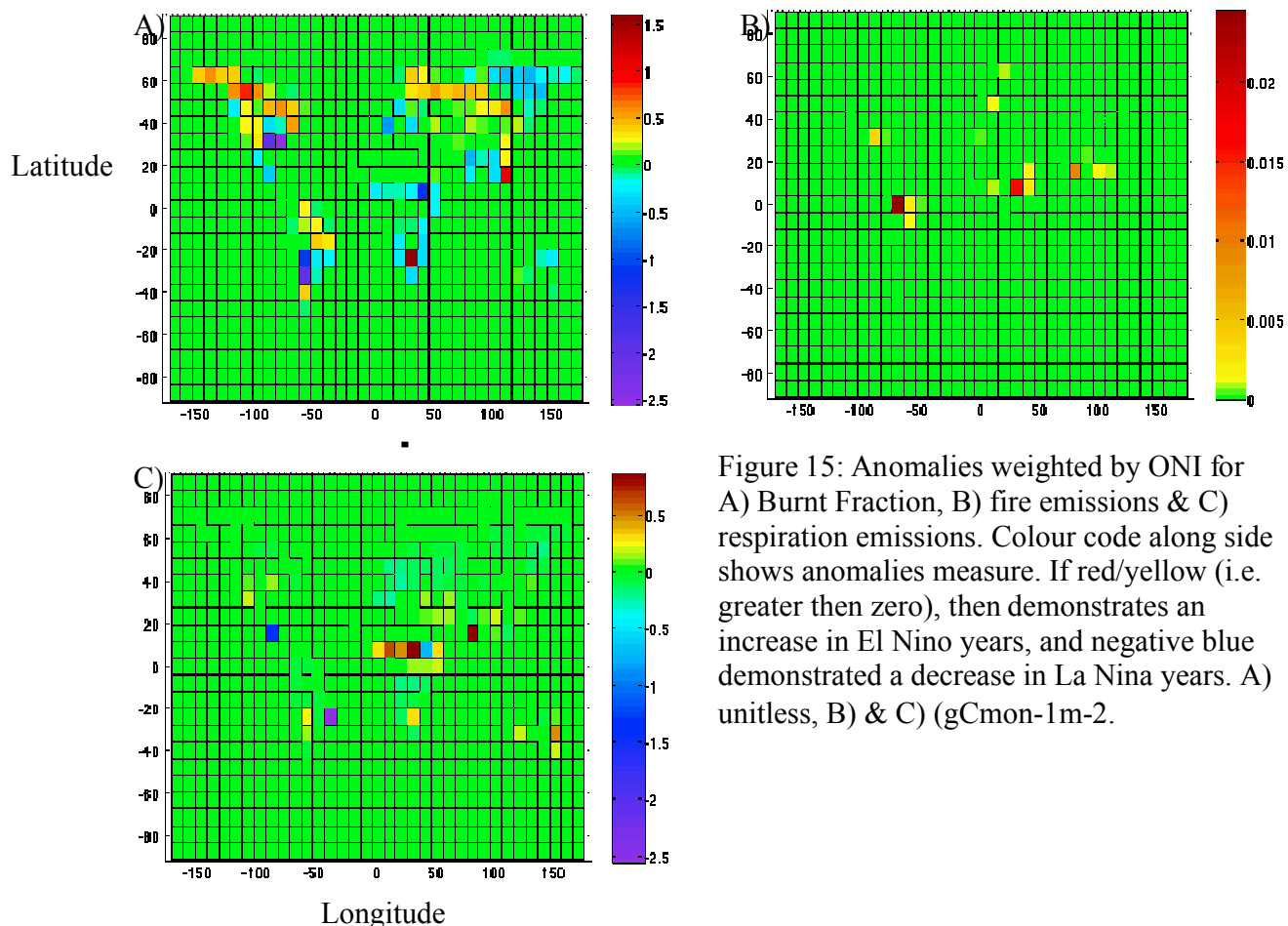


Figure 15: Anomalies weighted by ONI for A) Burnt Fraction, B) fire emissions & C) respiration emissions. Colour code along side shows anomalies measure. If red/yellow (i.e. greater than zero), then demonstrates an increase in El Niño years, and negative blue demonstrated a decrease in La Niña years. A) unitless, B) & C) (gCmon-1m-2).

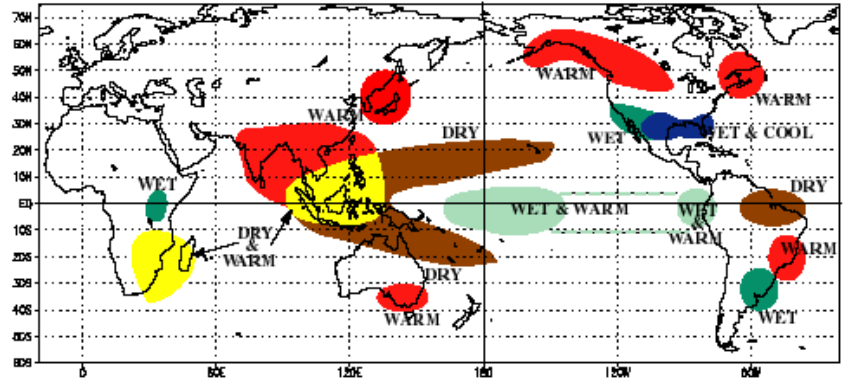
During El Niño years, emission from emissions database show significant correlation with El Niño events (van der Werf 2004 & 2006; figure 12), with an increase of 11% global emission for every 1 unit change in ONI. The study regions show exponential increases in fire emissions with INO index.

Figure 13, shows the modelled carbon emission from respirations and fire. In most El Niño years, both global emission tend to rise, although there is a stronger signal in fire carbon emissions, particularly at the end on the 90s. In the rainforest Niño study region, there also seems to be a drop in respiration fluxes during El Niño years, so all extra carbon emissions from these regions are as a result of fire. Although the current limitations in the model, discussed in model validation above (pg27-28), mean that quantitative analysis over relative contributions from respiration and fire emissions are meaningless at this stage, it is possible to qualitatively explore effects of El Niño on global fire regimes. To compare global effects on fire regime, figure 15 show burnt fraction, fire and respiration carbon emission anomalies weight by ONI:

$$\delta_{v,B} = \frac{1}{n_t} \sum_{t=1}^{n_t} \frac{(B_{sim} - \mu_{B,sim})}{ONI_t} \quad (20)$$

This demonstrates an increase in burnt fraction across central and Western Amazonian and South Asia during El Nino years, as well as parts of Western Russia and Eastern Europe. Siberian Coniferous forests show an increased sink during El Nino years, whilst coniferous and deciduous forests of North America have a diminished sink. It is worth noting the variability in burnt fraction in and around South America. The burnt fraction variational distribution is roughly what you'd expect from the climate variations associated with El Nino (figure 16).

WARM EPISODE RELATIONSHIPS DECEMBER - FEBRUARY



WARM EPISODE RELATIONSHIPS JUNE - AUGUST

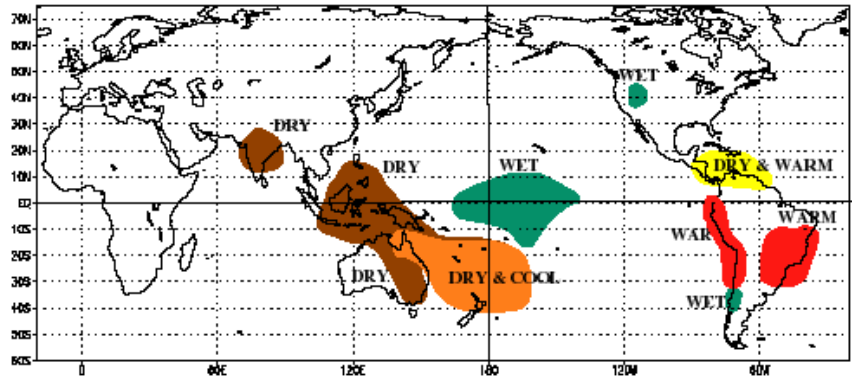


Figure 16, El Nino effects different parts of the terrestrial biosphere. Reproduced from <http://www.ngdc.noaa.gov/paleo/ctl/images/warm.gif>

6. Discussion and Conclusion

Although quantitative analysis of ENSO effects on various terrestrial carbon fluxes was not possible at this stage, the model was able to show qualitative spatial ENSO fluctuations, with variations that match the expected outcome from ENSO climate anomalies (figure 16). This demonstrated an increase in burnt fractions during ENSO positive phase in Tropical rainforests, a biome that is vulnerable, as it has evolved with a minimal fire regime (Sanford et al., 1985; Turcotte et al., 1998), and with large carbon stores, demonstrated by the substantial increase in fire carbon emissions in the Amazon region, both modeled and observed. However, some parts of the world show an increased sink in El Niño conditions (such as Siberian Russia). Depending on how ENSO and Climate changes in the future, an increase in drought conditions such as those associated with El Niño could have a substantial impact on the carbon cycle, and could result in a positive feedback (e.g., Amazon and other tropical areas) or negative (Siberian Russia) with the Carbon Cycle. Variations in other oscillations (such as the North Atlantic Oscillation) may also have important effects. Better understanding of future regional climate change, and alterations to oscillations such as ENSO, is therefore vital to understand how these interactions on the carbon cycle will change in the future.

For the continuation of the study, optimization through high resolution may yield more accurate results and, if not, allow better diagnostics as to what processes in the model do not describe accurately fire regimes or emissions. Also, incorporating uncertainties of processes and steps in FISSLING to add to the resulting Hessian will result in better understanding of the accuracy of the processes, and uncertainties (uncertainties from the Hessian were not considered in this study). After key processes have been properly constrained and tested, forward modeling, replacing BETHY observational inputs with that from a GCM, may help to understand how fire regimes may alter in the future.

After this study has concluded, it would be worth extending it to incorporate a model, or an adaptation to BETHY, for varying PFT compositions in grid cells. This could go some way to predict likely succession where fire regimes could change (such as the Amazon) and for other climate change related disturbances, and to see if changes in biomes, and thus big changes in terrestrial carbon stores, could occur.

References

- Albini, F.A. (1976) *Estimating wildfire behaviour and effects*. USDA Forest Service General Technical Report INT-30. Intermountain Forest and Range Experiment Station, Forest Service, U.S. Department of Agriculture, Ogden, Utah.
- Andreae, M.O. (1992) Biomass burning: its history, use, distribution and its impact on environmental quality and global climate. *Global biomass burning, atmospheric implications and biospheric implications* J.C. Levine), pp. 3–21. MIT Press, Cambridge, MA.
- Barber R.T, Chávez, F.P. (1986) Ocean variability in relation to living resources during the 1982–83 El Niño. *Nature* 319, 279 – 285
- Barbosa, P., Stroppiana, D., Grégoire, J.-M. & Pereira, J.M.C. (1999) An assessment of fire in Africa (1981–1991): burnt areas, burnt biomass and atmospheric emissions. *Global Biogeochemical Cycles*, 13, 933–950.
- Barrett, E.c. Curtis L.F. (1999), *Introduction to Enviromental Remote Sensing, 4th edition*, Stanley Thornes (Publishers) Ltd, Cheltenham.
- Battle, M., Bender, M.L., Tans,P.P., White, J.W.C., Ellis, J.T., Conway ,T., Francey, R.J. (2000) Global carbon sinks and their variability inferred from atmospheric O-2 and delta C-13, *Science*, **287**, 2467–2470.
- BOND, W J., MIDGLEY G.F., WOODWARD, F.I.,(2003) The importance of low atmospheric CO₂ and fire in promoting the spread of grasslands and savannas. *Global Change Biology* **9**, 973 – 982
- Bond, W.J., Woodward, F.I., Midgley, G.F. (2005) The global distribution of ecosystems in a world without fire. *New Phytologist*, **165**, 525-538.
- Bond-Lamberty, B., Wang, C., Gower, S.T. (2004) Net primary production and net ecosystem production of a boreal black spruce wildfire chronosequence. *Global Change Biology*, **10:4**, 473 - 487
- Bousquet, P., Peylin, P., Ciais, P., LeQuere, C., Friedlingstein, P., Tans, P.P. (2000) Regional changes in carbon dioxide fluxes of land and oceans since 1980, *Science*, **290**, 1342–1346.
- Brown, J.K. (1981) Bulk Densities of Nonuniform Surface Fuels and Their Application to Fire Modeling. *Forest Science*, **27**, 667-683.
- Burgan, R.E., Hartford ,R.A. (1996) *Live vegetation moisture calculated from NDVI* and used in fire danger rating. Thirteenth Conference on Fire and Forest Meteorology, Fairfield, WA: International Association of Wildland Fire, pp.225–231.
- Burgan, R.E., Klaver, R.W., Klaver, J.M. (1998) “Fuel Models and Fire Potential from Satellite and Surface Observations” *International Journal of Wildland Fire*, **8:3**, 159-170

Byron, N., Shepherd, G. (1998) *INDONESIA AND THE 1997-98 EL NIÑO: FIRE PROBLEMS AND LONG-TERM SOLUTIONS*, Commonwealth Forestry Review

Cahoon, D.R. Jr, Stocks, B.J., Levine, J.S., Cofer, W.R. III & O'Neill, P.O. (1992) Seasonal distribution of African savanna fires. *Nature*, **359**, 812–815.

CANE, M. A., 1986, El Ni no. *Annual Review o f Earth and Pl anet ary Sciences*, **1 4** , 4 3 - 7 0 .

Carrè, M., Bentaleb, I., Fontugne, M., Lavalée, D. (2005) Strong El Niño events during the early Holocene: stable isotope evidence from Peruvian sea shells. *The Holocene*, **15:1**, 42–47.

Chapin III, F.S., Walker, B.H., Hobbs, R.J., Hooper, D.U., Lawton J.H., Sala, O.E., Tilman, D. (1997) Biotic Control over the Functioning of Ecosystems. *Science* **277**, 500 – 504.

Chuvieco, E., Aguado, I., Dimitrakopoulos A.P. (2004) Conversion of fuel moisture content values to ignition potential for integrated fire danger assessment, *Can. J. For. Res.*, **34:11**, 2284-2293

Ciais, P., Reichstein, M., Viovy, N., Granier, A., Ogee, J., Allard, V. , Aubinet, M., Buchmann, N., Bernhofer, C., Carrara, A., Chevalier, F., DeNoblet, N., Friend, A.D., Friedlingstein, P., Grunwald, T., Heinesch, B., Keronen, P., Knohl, A., Krinner, G., Loustau, D., Manca, G., Matteucci, G., Miglietta, F., Ourcival, J.M., Papale, D., Pilegaard, K., Rambal, S., Seufert, G., Soussana, J.F., Sanz, M.J., Schulze, E.D., Vesala, T., Valentini, R. (2005) Europe-wide reduction in primary productivity caused by the heat and drought in 2003, *Nature*, **437**, 529–533.

Clark, D.A., Piper, S.C., Keeling, C.D., Clark, D.B. (2003) Tropical rain forest tree growth and atmospheric carbon dynamics linked to interannual temperature variation during 1984–2000, *Proc. Nat. Acad. Sci. USA*, **100:10**, 5852–5857

Cochrane, M.A., Schulze, M.D. (1999), Forest Fires in the Brazilian Amazon, *Conservation Biology*.

Collins, M. (2005) El Niño- or La Niña-like climate change?. *Climate Dynamics*, **24:1**, 89–104.

Conard S.G., Ivanova, G.A. (1997) Wildfire in Russian Boreal Forests—Potential Impacts of Fire Regime Characteristics on Emissions and Global Carbon Balance Estimates. *Environmental Pollution*, **98:3**, 305-313

Cox, P.M., Betts, R.A., Collins, M., Harris, P.P., Huntingford, C., Jones, C.D. (2004) Amazonian forest dieback under climate-carbon cycle projections for the 21st century. *Theoretical and Applied Climatology*, **78**, 137-156

“CCDAS.org”, <http://www.ccdas.org>, viewed: 16/01/08

Denman K. L., Brasseur G. et al (2007) *Couplings Between Changes in the Climate System and Biogeochemistry. IPCC Fourth Assessment Report: Working Group I Report "The Physical Science Basis"*, (ed. by Houghton J T et al) pg499-588, Cambridge Univ. Press, Cambridge, UK,

Dennison, P.E., Roberts, D.A., Peterson, S.H., Rechel, J. (2005) Use of Normalized Difference Water Index for monitoring live fuel moisture. *International Journal of Remote Sensing* **26:5**, 1035 — 1042

DIAZ, H. F., and MARKGRAF, V., 1993, Introduction. In *El Niño: Historical and Paleoclimatic Aspects of the Southern Oscillation* (ed. by Diaz H.F., Markgraf, V.) pp. 1-14. New York: Cambridge University Press

Di Bella, C.M., Jobbágy, E.G., Paruelo, J.M. Pinnock, S. (2006) Continental fire density patterns in South America. *Global Ecology & Biogeography* **52:2** 192-199

Dwyer, E., Pinnock, S., Grégoire, J.-M. & Pereira, J.M.C. (2000) Global spatial and temporal distribution of vegetation fire as determined from satellite information. *International Journal of Remote Sensing*, **21**, 1289–1302.

GHCN-Monthly version 2 (2008) <ftp://ftp.ncdc.noaa.gov/pub/data/ghcn/v2>, National Environmental Satellite, Data and Information Services, NOAA CMDL, Boulder, Colorado.

Giglio, L., Descloitres, J., Justice, C. O., Kaufman, Y. J. (2003) An enhanced contextual fire detection algorithm for MODIS, *Remote Sens. Environ*, **87**, 273–282.

Giglio, L., van der Werf, G. R., Randerson, J. T., Collatz, G. J., Kasibhatla, P. S. (2006) Global estimation of burned area using MODIS active fire observations, *Atmos. Chem. Phys.*, **6**, 957–974.

GLANTZ, M., 1991, Introduction. In *Teleconnections Linking World Wide Climate Anomalies: Scientific Basis and Societal Impact*, (ed. by Glantz, M.H., Kat R.H., Nicholls N.), pp. 1-12. New York: Cambridge University Press

GLOBALVIEW-CO2 (2001) *Cooperative Atmospheric Data Integration Project - Carbon Dioxide*, CD-ROM, NOAA CMDL, Boulder, Colorado, [Also available on Internet via anonymous FTP to <ftp.cmdl.noaa.gov>, Path: <cgg/co2/GLOBALVIEW>].

Goulden, M.L., Munger, J.W., Fan, S.M., Daube, B.C., Wofsy, S.C. (1996) Exchange of carbon dioxide by a deciduous forest: Response to interannual climate variability, *Science*, **271**, 1576–1578.

Grace, J., Malhi, Y., Higuchi, N., Meir, P. (2001) *Terrestrial Global Productivity: Past, Present, and Future*. (ed. by Moone, H. A., Roy, J., Saugier, B.). London: Academic. pp. 401–428.

Hao, W.-M., Liu, M.-H., Crutzen, P. J. (1990) *Estimates of annual and regional releases of CO2 and other trace gases to the atmosphere from fires in the tropics, based on the FAO statistics for the period 1975-1980*, in: *Fire in the Tropical Biota: Ecosystem Processes and Global Challenges*, (ed. by Goldammer, J. G.) pp. 400–462, Springer-Verlag, New York, 1990.

Haugaasen, T., Barlow, J., Peres C.A. (2003) Surface wildfires in central Amazonia: short-term impact on forest structure and carbon loss. *Forest Ecology and Management*, **179**, 321-331

Heimann, M. (1995) *The global atmospheric tracer model TM2, Technical Report No. 10*, Max-Planck-Institut für Meteorologie, Hamburg, Germany.

- Hobbs, R.J., Arico, S., Aronson, J., Baron, J.S., Brigewater, P., Cramer, V.A., Epstein, P.R., Ewel, J.J., Klink, C.A., Lugo, A.E., Norton, D., Ojima, D., Richardson, D.M., Sanderson, E.W., Valladares, F., Vila, M., Zomora, R. (2006) Novel ecosystem: theoretical and management aspects of the new ecological world order. *Global Ecol. Biogeogr.*, **15**, 1-7.
- Hoffa, E.A., Ward, D.E., Hao, W.M., Susott, R.A., Wakimoto, R.H. (1999) Seasonality of carbon emissions from biomass burning in a Zambian savanna, *J. Geophys. Res.-Atmos.*, **104**, 13841–13853.
- Holdsworth, A.R., Uhl, C. (1997) Fire in Amazonian selectively logged rain forest and the potential for fire reduction, *Ecological Applications*, **7:2**, 713-725
- JIANHUA J.U., SLINGO, J. (1995) The Asian summer monsoon and ENSO, *Quarterly Journal of the Royal Meteorological Society*, **121**, 1133-1168
- Jones, C.D. & Cox, P.M. (2005) On the significance of atmospheric CO₂ growth rate anomalies in 2002–2003, *Geophys. Res. Lett.*, **32**, L14816
- Jonas, M., Nilsson, S., Shvidenko, A., Stolbovoi, V., Gluck, M., Obersteiner M., Oeskog, A. (1999), *Full Carbon Accounting and the Kyoto Protocol: A Systems- Analytical View*. International Institute for Applied Systems Analysis: Working paper ir99025
- Justice, C., Dowty, P. (1994) *IGBP-DIS satellite fire detection algorithm workshop technical report*. IGBP-DIS working paper no. 9, p. 88, February 1993. NASA/GSFC, Greenbelt, MD.
- Kaminski, T., Heimann, M., Giering, R. (1999) A coarse grid three dimensional global inverse model of the atmospheric transport, 1, Adjoint model and Jacobian matrix. *J. Geophys. Res.*, **104**, 18,535–18,553.
- Kaminski, T., Knorr, W., Rayner, P., Heimann, M. (2002) Assimilating atmospheric data into a terrestrial biosphere model: A case study of the seasonal cycl. *Global Biogeochemical Cycles*, **16**, 14–1–14–16..
- Kaminski, T., Giering, R., Scholze, M., Rayner, P., Knorr, W. (2003) *An example of an automatic differentiation-based modelling system, in Computational Science – ICCSA 2003, International Conference Montreal, Canada, May 2008, Proceedings, Part II* (ed. by Kumar, V., Gavrilova, L., Tan, C. J. K., L'Ecuyer, P.) vol. 2668 of Lecture Notes in Computer Science, pp. 95–104, Springer, Berlin.
- Keane, R.E., Morgan, P. & Running, S.W. (1996) *FIRE-BGC — a mechanistic ecological process model for simulating fire succession on coniferous forest landscapes of the Northern Rocky Mountains*. Research Paper INT-RP-484. USDA Forest Service Intermountain Research Station, Ogden, Utah
- Keeling, C.D., Bacastow, R.B., Carter, A.F., Piper, S.C., Whorf, T.P., Heimann, M., Mook, W.G., Roeloffzen, H., *A three-dimensional model of atmospheric CO₂ transport based on observed winds: 1. Analysis of observational data*, in AGU Monograph, pp. 277-303, American Geophysical Union, Washington D. C., 1989.

Kitzberger, T. & Veblen, T.T. (1997) Influences of humans and ENSO on fire history of *Austrocedrus chilensis* woodlands in northern Patagonia, Argentina. *Ecoscience*, **4**, 508–520.

Knorr, W., (1997) *Satellitengestützte Fernerkundung und Modellierung des Globalen CO₂-Austauschs der Landvegetation: Eine Synthese*, Ph.D. thesis, Max-Planck-Institut für Meteorologie, Hamburg, Germany.

Knorr W, (2000) Annual and interannual CO₂ exchanges of the terrestrial biosphere: process based simulations and uncertainties. *Global Ecology and Biogeography*, **9**, 225-252.

Knorr, W., Schulz, J.P. (2001) *Using satellite data assimilation to infer global soil moisture and vegetation feedback to climate*, in *Remote Sensing and Climate Modeling: Synergies and Limitations*, (ed. by Beniston, M., Verstraete, M.) Advances in Global Change Research, pp. 273–306, Kluwer Academic Publishers, Dordrecht, the Netherlands.

Knorr, W., Gobron, N., Scholze, M., Kaminski, T., Pinty, B. (2005b) Global-scale drought caused atmospheric CO₂ increase. *EOS Transactions*, **86:18**,178-181.

Knorr, W., Gobron, N., Scholze, M., Rayner, P., Kaminski, T., Giering, R., Widmann, H., Kattge, J. (2005c) *Carbon and fAPAR assimilation within CCDAS* (ed. by Viterbo P.) Proceedings of ECMWF/ELDAS Workshop on Land Surface Assimilation, 8-11 November 2004, pages 213-219. European Centre for Medium-Range Weather Forecasts.

Kyoto Protocol, (1998), *Kyoto Protocol to the United Nations Framework Convention on Climate Change*, http://unfccc.int/essential_background/kyoto_protocol/items/1678.php, date visited: 14/01/09

¹ Jonas, M. et al, (1999), "Full Carbon

Langenfelds, R.L., Francey, R.J., Pak, B.C., Steele, L.P., Lloyd, J., Trudinger, C.M., Allison, C.E. (2002) Interannual growth rate variations of atmospheric ¹³C₂O and its C, H₂, CH₄, and CO between 1992 and 1999 linked to biomass burning, *Global Biogeochem. Cycles*, **16:3**, 1048-1069.

Last of the Wild Data Version 2, 2005 (LWP-2): *Global Last of the Wild (LTW)*. Wildlife Conservation (WCS) and Center for International Earth Science Information Network (CIESIN).

Latif, M., Grotzner, A. (2000) The equatorial Atlantic oscillation and its response to ENSO. *Earth and Environmental Science*, **16**, 213-218

Lee, K., Wanninkhof, R., Takahashi, T., Doney, S.C., Feely, R.A. (1998) Low interannual variability in recent oceanic uptake of atmospheric carbon dioxide. *Nature*, **396**, 155–159

Leeper, G.W., Uren, N.C. (1993). *Soil science, an introduction, 5th edn*, Melbourne: Melbourne University Press.

Levine, J.S., ed. (1991) *Global biomass burning: atmospheric, climatic, and biospheric implications*. MIT Press, Cambridge, MA.

Loreau, L., Naeem, S., Inchausti, P., Bengtsson, J., Grime, J.P., Hector, A., Hooper, D.U., Huston, M.A., Raffaelli, D., Schmid, B., Tilman, D., Wardle, D.A. (2001), Biodiversity and Ecosystem Functioning: Current Knowledge and Future Challenges. *Science*, 294: 5543, 804 - 808

Lyon, B., (2004) The strength of El Niño and spatial extent of tropical drought, *Geophys. Res. Lett.*, **31**, L21204, doi:10.1029/2004GL020901

MacKay G., Naeem, J., (1984), Forest fires as critical phenomena. *J. Phys. A: Math. Gen.* **17**, pg757-760.

Mark G. L., Nieuwstadt, V., Sheil, D (2004) Drought, fire and tree survival in a Borneo rain forest, East Kalimantan, Indonesia. *Journal of Ecology*, **93:1**, 191 – 201

Merryfield, W. J. (2006). Changes to ENSO under CO₂ Doubling in a Multimodel Ensemble. *Journal of Climate* **19:16**: 4009–4027

MODIS/Aqua Thermal Anomalies/Fire Daily L3 Global 1km SIN Grid V005, obtained from: <ftp://e4ftl01u.ecs.nasa.gov/MOLA/MYD14A1.005/>

Nair R. D., Côté, J., Staniforth, A. (1999): Cascade interpolation for semi-Lagrangian advection over the sphere. *Quart. J. Roy. Meteor. Soc.*, **125**, 1445–1468.

Narayan C., Fernandes, P.M., van Brusselen, J., Schuck A. (2007) Potential for CO₂ emissions mitigation in Europe through prescribed burning in the context of the Kyoto Protocol. *Forest Ecology and Management*, **251:3**, 164-173

Nesterov VG (1949) Gorimost' lesa i metody eio opredelenia . Goslesbumaga Moscow.

Nelson, B.W. (1994) Natural forest disturbance and change in the Brazilian Amazon. *Remote Sensing Reviews*, **10**, 105–125.

Norby, R.J., DeLucia, E.H., Gielen, B, Calfapietra, C., Giardina, C.P., King, J.S., Ledford, J., McCarthy, H.R., Moore, D.J.P., Ceulemans, R., Angelis, P.D., Finzi, A.C., Karnosky, D.F., Kubiske, M.E., Lukac, M., Pregitzer, K.S., Scarascia-Mugnozza, G.E., Schlesinger, W.H., Oren R. (2005) Forest response to elevated CO₂ is conserved across a broad range of productivity. *Proceedings of the National Academy of Sciences*, **102**, 18052-18056.

Olson, D.M., Dinerstein, E., Wikramanayake, E.D., Burgess, N.D., Powell, G.V.N., Underwood, E.C., D'amico, J.A., Itoua, I., Strand, H.E., Morrison, J.C., Loucks, C.J., Allnutt, T.F., Ricketts, T.H., Kura, Y., Lamoreux, J.F., Wettengel,

W.W., Hedao, P., Kassem K.R., (2001). Terrestrial Ecoregions of the World: A New Map of Life on Earth. *BioScience*, **51:11**, 933-938

Pereira, J. M., Pereira, B. S., Barbosa, P., Stroppiana, D., Vasconcelos, M. J. P., Grégoire, J.-M. (1999) Satellite monitoring of fire in the EXPRESSO study area during the 1996 dry season experiment: Active fires, burnt area, and atmospheric emissions, *J. Geophys. Res.-Atmos.*, **104**, 30 701–30 712.

Pidwirny, M., Draggan S., McGinley, M. (2007) *Terrestrial biome*. In: Encyclopedia of Earth. (eds by Cleveland C.J. [First published in the Encyclopedia of Earth October 17, 2006; Last revised December 4, 2007; Retrieved September 21, 2008]. <http://www.eoearth.org/article/Terrestrial_biome>

Prentice, C.I., Guiot, J., Huntley B., Jolly D. Cheddadi, R., (1996) *Reconstructing biomes from palaeoecological data: a general method and its application to European pollen data at 0 and 6 ka*, *Climate Dynamics*, **12**, 185-194

Randerson, J. T., G. R. van der Werf, L. Giglio, G. J. Collatz, and P. S. Kasibhatla. 2007. *Global Fire Emissions Database, Version 2 (GFEDv2.1)*. Data set. Available on-line [<http://daac.ornl.gov/>] from Oak Ridge National Laboratory Distributed Active Archive Center, Oak Ridge, Tennessee, U.S.A. doi:10.3334/ORNLDAAC/849.

Rayner, P., Scholze, M., Knorr, W., Kaminski, T., Giering, R., Widmann, H. (2005), Two decades of terrestrial carbon fluxes from a Carbon Cycle Data Assimilation System (CCDAS). *Global Biogeochemical Cycles*, **19**, doi:10.1029/2004GB002,254

Rasmusson, E.M. (1985) El-Nino and variations in climate. *american scientist*, **73:2**, 168 -177

Rasmusson, E.M. Wallace, J.M. (1983) Meteorological Aspects of the El Niño/Southern Oscillation. *Science*, **222**, 1195-1202

Sanderson, E.W., Jaiteh, M., Levy, M.A., Redford, K.H., Wannebo, A.V., Woolmer, G. (2002) The Human Footprint and the Last of the Wild. *BioScience*, **52:10**, 891-904

Scholze, M. (2003) *Model studies on the response of the terrestrial carbon cycle on climate change and variability*, Examensarbeit, Max-Planck-Institut für Meteorologie, Hamburg, Germany.

Schultz, J. (1988) *Die Ökozonen der Erde: die Ökologische Gliederung der Geosphäre*. Ulmer, Stuttgart.

Seiler, W., Crutzen, P. J. (1980) Estimates of gross and net fluxes of carbon between the biosphere and atmosphere from biomass burning, *Climate Change*, **2**, 207–247.

Sims, D.A., GAMON, J.A. (2003) Estimation of vegetation water content and photosynthetic tissue area from spectral reflectance: a comparison of indices based on liquid water and chlorophyll absorption features. *Remote Sensing of Environment*, **84**, 526–537.

Shvidenko, A., Nilsson, S., Roshkov, V. (1995) *Possibilities for Increased Carbon Sequestration through Improved Protection of Russian Forests*. IIASA Working Paper WP-95-086, pp 28, IIASA

- Trenberth, K. E.; Caron, J.M., Stepaniak, D.P., Worley, S. (2002) Evolution of El Niño – Southern Oscillation and global atmospheric surface temperatures. *Journal of Geophysical Research*, **107**, D84065. doi:10.1029/2000JD000298.
- Thonicke, K., Spessa, A., Prentice, I.C. Model description of SPread and InTensity of FIRE (SPITFIRE), unpublished
- Thonicke, K., Venevsky, S., Sitch, S., Cramer, W. (2001) The role of fire disturbance for global vegetation dynamics: coupling fire to a Dynamic Global Vegetation Model. *Glob. Ecol. and Biogeogr.*, **10**, 661-677
- Trunfio, G.A., (2004) *Predicting Wildfire Spreading Through a Hexagonal Cellular Automata Model*, Lecture Notes in Computer Science: Cellular Automata, 385-394
- Turner, D. P., Guzy, M., Lefsky, M. A., Ritts, W. D., Tuyl, S. van, Law, B. E. (2004) Monitoring forest carbon sequestration with remote sensing and carbon cycle modeling. *Environmental Management*, **33:4**, 457-466
- van der Werf, G.R., Randerson, J.T., Collatz, G.J., Giglio, L., Kasibhatla, P.S., Arellano Jr, A.F., Olsen, S.C., Kasischke, E.S. (2004) Continental-Scale Partitioning of Fire Emissions During the 1997 to 2001 El Niño/La Niña Period, *Science*, **203**, 73-76
- Van der Werf, G. R., Randerson, J.T., Giglio, L., Collatz, G.J., Kasibhatla, P.S. (2006). Interannual variability in global biomass burning emission from 1997 to 2004, *Atmospheric Chemistry and Physics*, **6**, 3423-3441.
- Vecchi G.A., Harrison D.E. (2000) Tropical Pacific sea surface temperature anomalies, El Niño, and equatorial westerly wind events. *Journal of Climate*, **13**, 1814-1830
- Viegas, D.X. (1997) *Modelling surface-fire behaviour. Forest fire risk and management* (ed. by European Commission), pp. 65–80. Office for Official Publications of the European Community, L-2985 Luxembourg.
- Wiedinmyer, C., Neff, J.C. (2007) Estimates of CO₂ from fires in the United States: implications for carbon management. *Carbon Balance Manag.*, **2:10**, doi: 10.1186/1750-0680-2-10.
- Williamson, B.G., Laurance, W.F., Oliveira, A.A., Delamônica, P., Gascon, C., Lovejoy, T.E. Pohl L. (2001) Amazonian Tree Mortality during the 1997 El Niño Drought. *Conservation Biology*, **14:5**, 1538-1542
- Wooster, M.J., Ceccato, P. and Flasse, S.P. (1998) Indonesian fires observed using AVHRR, *Int. J. Rem. Sens.*, **19**, 383-386.
- Zeng, N., Mariotti, A., Wetzal, P. (2005) Terrestrial mechanisms of interannual CO₂ variability, *Global Biogeochemical Cycles*, **19**, doi:10.1029/2004GB002273.

